

Analysis of EDZ Development of Columnar Jointed Rock Mass in the Baihetan Diversion Tunnel

Xian-Jie Hao¹ · Xia-Ting Feng¹ · Cheng-Xiang Yang² · Quan Jiang¹ · Shao-Jun Li¹

Received: 29 October 2014 / Accepted: 21 August 2015 / Published online: 1 September 2015
© Springer-Verlag Wien 2015

Abstract Due to the time dependency of the crack propagation, columnar jointed rock masses exhibit marked time-dependent behaviour. In this study, in situ measurements, scanning electron microscope (SEM), back-analysis method and numerical simulations are presented to study the time-dependent development of the excavation damaged zone (EDZ) around underground diversion tunnels in a columnar jointed rock mass. Through in situ measurements of crack propagation and EDZ development, their extent is seen to have increased over time, despite the fact that the advancing face has passed. Similar to creep behaviour, the time-dependent EDZ development curve also consists of three stages: a deceleration stage, a stabilization stage, and an acceleration stage. A corresponding constitutive model of columnar jointed rock mass considering time-dependent behaviour is proposed. The time-dependent degradation coefficient of the roughness coefficient and residual friction angle in the Barton–Bandis strength criterion are taken into account. An intelligent back-analysis method is adopted to obtain the unknown time-dependent degradation coefficients for the proposed constitutive model. The numerical modelling results are in good agreement with the measured EDZ. Not only that, the

failure pattern simulated by this time-dependent constitutive model is consistent with that observed in the scanning electron microscope (SEM) and in situ observation, indicating that this model could accurately simulate the failure pattern and time-dependent EDZ development of columnar joints. Moreover, the effects of the support system provided and the in situ stress on the time-dependent coefficients are studied. Finally, the long-term stability analysis of diversion tunnels excavated in columnar jointed rock masses is performed.

Keywords Columnar jointed rock mass · Excavation damaged zone · Time-dependent behaviour · Long-term stability

Abbreviations

C_0	Cohesion of the basalt rock (MPa)
C_{j3}	Cohesion of the horizontal joint inside a column (MPa)
$d\sigma$	Stress increment (MPa)
E_1	Elastic moduli of the basalt perpendicular to the column axis (GPa)
E_2	Elastic moduli of the basalt parallel to the column axis (GPa)
f_{j1}^s	Shear criterion of joint between columns (MPa)
f_{j1}^t	Tension criteria of joint between columns (MPa)
f_{j2}^s	Shear criterion of plumose joint inside a column (MPa)
f_{j2}^t	Tension criteria of plumose joint inside a column (MPa)
f_{j3}^s	Shear criteria for the horizontal joint inside a column (MPa)
f_{j3}^t	Tension criteria for the horizontal joint inside a column (MPa)

✉ Xia-Ting Feng
xtfeng@whrsm.ac.cn; xia.ting.feng@gmail.com

¹ State Key Laboratory of Geomechanics and Geotechnical Engineering, Institute of Rock and Soil Mechanics, Chinese Academy of Sciences, Wuhan 430071, Hubei, People's Republic of China

² School of Resources and Civil Engineering, Northeastern University, Shenyang 110004, People's Republic of China

G	Shear modulus of the basalt (GPa)	τ_{j2}	Shear stress on the plumose joint inside a column (MPa)
h_{j3}	Shear-tensile boundary mixed criteria for the horizontal joint inside a column (MPa)	τ_{j3}	Shear stress on the horizontal joint inside a column (MPa)
JCS^{j1}	Joint wall compressive strength of joint between columns (MPa)	ν_1	Poisson's ratio of the basalt perpendicular to the column axis
JCS^{j2}	Joint wall compressive strength of plumose joint inside a column (MPa)	ν_2	Poisson's ratio of the basalt parallel to the column axis
JRC^{j1}	Joint roughness coefficient of joint between columns		
JRC^{j2}	Joint roughness coefficient of plumose joint inside a column		
$[K]$	Global stiffness matrix (MPa)		
K_{JRC}	Time-dependent degradation coefficients of joint roughness coefficient		
K_{ϕ_r}	Time-dependent degradation coefficients of residual friction angle		
$[R^i]$	Transformation matrix of the i th set of joint planes (MPa)		
r	Tunnel radius (m)		
δ	Wall displacement of tunnel (mm)		
ϕ_0	Internal friction angle of the basalt ($^\circ$)		
ϕ_{j3}	Internal friction angle of the horizontal joint inside a column ($^\circ$)		
ϕ_m^{j1}	Friction angle considering dilatancy effects of joint between columns ($^\circ$)		
ϕ_m^{j2}	Friction angle considering dilatancy effects of plumose joint inside a column ($^\circ$)		
ϕ_r^{j1}	Residual friction angle of joint between columns ($^\circ$)		
ϕ_r^{j2}	Residual friction angle of plumose joint inside a column ($^\circ$)		
$\sigma_{3/3'}^{j1}$	Normal stress on the joint between columns (MPa)		
$\sigma_{3/3'}^{j2}$	Normal stress on the plumose joint inside a column (MPa)		
$\sigma_{3/3'}^{j3}$	Normal stress on the horizontal joint inside a column (MPa)		
σ_{j1}^t	Tensile strength of joint between columns (MPa)		
σ_{j2}^t	Tensile strength of plumose joint inside a column (MPa)		
σ_{j3}^t	Tensile strength of the horizontal joint inside a column (MPa)		
σ_t	Tensile strength of the basalt rock (MPa)		
ε	Strain tensor of the columnar jointed rock mass (MPa)		
ε^I	Strain tensor of the intact rock (MPa)		
ε^J	Strain tensor of the joints (MPa)		
ε_a	Threshold strain that rock mass entered an acceleration stage (mm/m)		
ε_s	Threshold strain that rock mass entered a stabilization stage (mm/m)		
ε_t	Tunnel strain (mm/m)		
τ_{j1}	Shear stress on the joint between columns (MPa)		

1 Introduction

Columnar joints are formed by the condensation of unexposed magma from volcanic eruptions. They are more developed in basalt (Spry 1962; Müller 1998). Columnar joints often display conspicuous bands oriented normal to the column axes, which are formed by contraction of cooling solidified magma (Lachenbruch 1962; Goehring et al. 2006). Due to the regularity of the block arrangements, large-scale basalt formations often become famous tourist attractions, such as the Giant's Causeway in Northern Ireland (see Fig. 1a); Fingal's cave on Staffa, Scotland; the Giant Column in Tengchong, Yunnan Province, China; and the submarine columnar joints of the Penghu Islands, Taiwan and Daepo Jusangjeolli on Cheju Island, South Korea. In recent years, many large hydropower stations have been built in southwest China. Some hydropower stations, such as Tongjiezi, Xiluodu, and Baihetan, have revealed different extents of development in the columnar joints encountered. Heavily developed joints have been found in columnar jointed rock masses in Baihetan (Fig. 1b), where the joint spacing is about 0.152 m on average (Jiang et al. 2014). According to the geological strength index (GSI) proposed by Hoek and Brown (1997) and Hoek (1998), such rock masses belong to the type referred to as "very blocky structures". The significant development of such joint leads to the columnar jointed rock mass easily collapsing after excavation if not supported in time (Fig. 2). Thus, the stability of the columnar jointed rock mass is one of the important problems facing tunnel excavation for the Baihetan hydropower stations.

Many researchers have investigated the stability of columnar jointed rock masses. The Basalt Waste Isolation Project (BWIP) focused on columnar jointed basaltic rock masses and was carried out in the USA in the 1980s (Côme et al. 1984; Cramer et al. 1987). Cundall (1988) and Hart et al. (1988) analysed columnar jointed rock masses for the BWIP using a simplified hexagonal cylindrical model. Through acoustic velocity and attenuation data, King et al. (1986) found that columnar jointed rock masses were

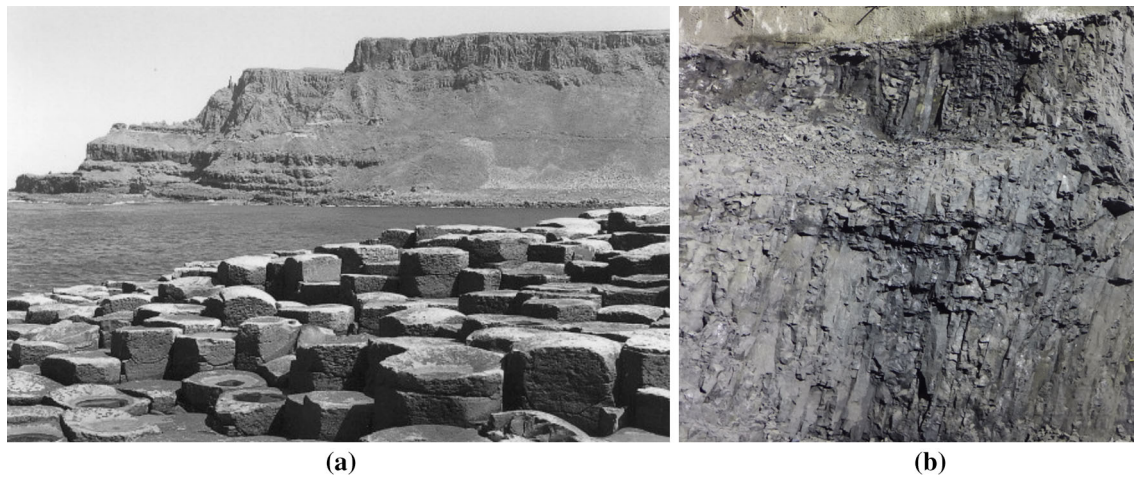


Fig. 1 Columnar jointed rock masses **a** Giant's Causeway, Northern Ireland (James 2009), and **b** Columnar joints at a diversion tunnel in Baihetan



Fig. 2 Collapse of columnar joints at a diversion tunnel in Baihetan

anisotropic, with a greater intensity of jointing along the horizontal rather than the vertical direction. Sitharam et al. (2001) proposed an equivalent continuum model for the estimation of jointed rock mass properties from the properties of intact rock, and a joint factor to evaluate stability that integrated all joint properties to account for joint frequency, orientation, and strength. Jiang et al. (2014) analysed the mechanical anisotropy of columnar jointed basalts, including aspects of the geometrical rock structure, and their deformation and strength anisotropy. Hatzor et al. (2015) studied the extent of the loosening zone in columnar basalts whose anisotropy presented a challenge for rock bolting design based on existing empirical criteria.

Due to the extensive development of the joints and the time dependency of crack propagation, columnar jointed rock masses not only have a large immediate excavation damaged zone (EDZ), but also have a time-dependency

EDZ. Even after a few months of the completion of excavation, the crack propagation and the depth of the EDZ in a columnar jointed rock mass still increase, which may lead to collapse of it. It can be seen that these time-dependent behaviours are important characteristics for columnar jointed rock masses. Therefore, an understanding of the time-dependent EDZ evolution behaviour in columnar jointed rock masses is of great significance to engineers assessing their stability. Despite this, so far, it has not been studied.

The evolution of an EDZ is influenced by several factors such as ground stress, geological conditions, the shape and size of the tunnel (Hudson et al. 2009). Many studies have been conducted, using various methods, regarding this topic. Traditionally, the most common method is an empirical method with in situ measurement data. All empirical functions can be shown to be related to the creep rate (Sakurai 1978). Another method, laboratory testing, was developed to observe the evolution process of the EDZ, such as: trap door tests (Park et al. 1999), the centrifuge model (Kamata and Masimo 2003), and small-scale models (Chambon and Corte 1994). There are also analytical methods used to study this topic (Sulem et al. 1987; Fahimifar et al. 2010; Nomikos et al. 2011).

Unfortunately, in spite of the significance of the aforementioned methods, they cannot be effectively used to comprehensively research all of the factors influencing the development of the EDZ. To overcome this difficulty, many numerical models have been developed to study the development of EDZs over time. For example, Hommand-Etienne et al. (1998) proposed a continuum damage constitutive law to reproduce the observable characteristics of the damaged zones. Eberhardt (2001) presented a 3D FEM analysis, where the progressive accumulation of damage is

correlated to irreversible elasto-plastic yielding. Kemeny (2003) developed a model for the time-dependent degradation of joint cohesion to illustrate the importance of time dependence in brittle fractured rock. Golshani et al. (2007) used an extended micromechanics-based damaged model considering time-dependent behaviour to analyse the development of the EDZ. Hudson et al. (2009) described the current knowledge regarding the thermo-hydro-mechanical-chemical modelling of the EDZ around the excavation of an underground radioactive waste repository. Rutqvist et al. (2008) modelled the damage, permeability changes, and pressure responses during the excavation of the TSX tunnel at the Underground Research Laboratory (URL, Canada). Pellet et al. (2009) presented a 3D numerical simulation of the mechanical behaviour of deep underground galleries with a special emphasis on the time-dependent development of the EDZ using a damageable visco-plastic constitutive law. Glamheden and Hökmark (2010) found that the creep rate is not only a function of the shear stress to shear strength ratio, but also of the absolute values of the shear and normal stresses by studying creep in jointed rock masses.

Basalt rock, in which columnar joints usually develop, is not prone to creep deformation as it is a hard rock. However, in columnar jointed rock masses, there are numerous joints, which are likely to open and crack after excavation. Therefore, crack propagation frequently occurs in such columnar jointed rock masses. To verify this, and analyse their time-dependent mechanical behaviour, borehole camera investigation and ultrasonic P-wave velocity tests are performed to observe the joint opening and crack propagation behaviour in the columnar jointed rock masses.

Therefore, in the present study, a time-dependent strength model for columnar joints is proposed. In which, the time-dependent degradation coefficient of the strength parameters is taken into account. The second section of this

research introduces the study area, in which we focus on the project geology, i.e. the columnar joint distribution in the diversion tunnel, the ground stress, the tunnel shape and size, the excavation method and its support scheme, etc. In the third section, the geometrical features of columnar joints are investigated. Then, the failure mechanism of each type of joint is studied by scanning electron microscopy (SEM). After that P-wave velocity measurements and borehole camera are then used to investigate the evolution of crack propagation and the time dependency of the EDZ in columnar joints, and three stages of EDZ development are proposed. A time-dependent strength model considering multiple joints and anisotropy characteristic is proposed in the fourth section and the time-dependent degradation coefficient of the strength parameters is obtained by back-analysis in the fifth section. The numerical simulation results are compared with in situ data. Finally, the influence of in situ stress on the time-dependent degradation coefficient for EDZ development and the long-term behaviour of the tunnel's stability are discussed.

2 Diversion Tunnels in a Columnar Jointed Rock Mass

2.1 General Project Information

The Baihetan hydropower station is located in the downstream reach of the Jinsha River. The left bank of the river belongs to Ningnan County, Sichuan Province, and the right bank to Qiaojia County, Yunnan Province (Fig. 3). The Baihetan hydropower station has a controlled watershed area of 430,300 km², a design normal storage water level of 825 m, a crest elevation of 834 m, a total reservoir capacity of 20.627 billion m³, a regulating capacity of 10.436 billion m³, a flood control capacity of 7.5 billion m³, a tentative installed capacity of 16,000 MW, and an

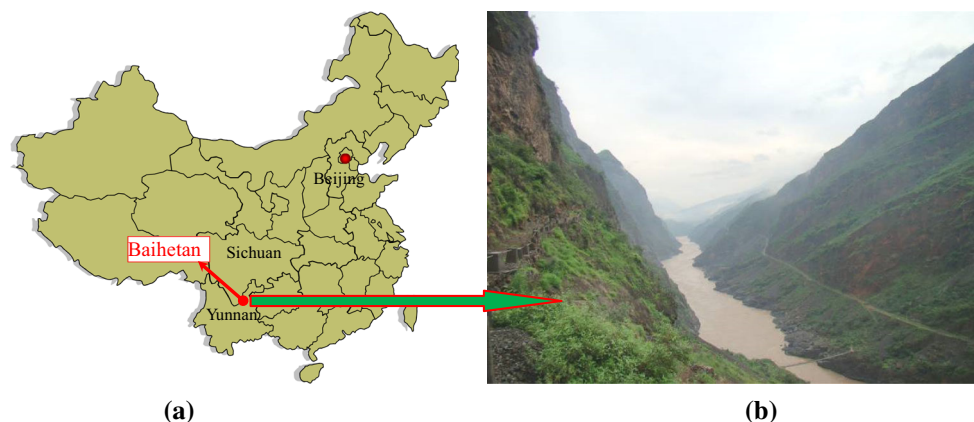


Fig. 3 **a** Location of Baihetan hydropower station and **b** its V-shaped valley landform

annual average generating capacity of 64.095 billion kW h. The Baihetan hydropower station is another 10 GW grade, giant hydropower project, for China, second only to the Three Gorges project.

2.2 Geological Setting

The valley of the Baihetan hydropower station is a typical asymmetric V-shape as shown in Fig. 3. Five diversion tunnels are used in its construction: three on the left bank and two on the right bank. From left to right, the tunnels are successively numbered 1–5, as shown in Fig. 4.

The strata around the diversion tunnels contain $P_2\beta_2^2$, $P_2\beta_3^3$, $P_2\beta_3$, $P_2\beta_4$, and $P_2\beta_5$ rock flow layers (Fig. 5). The rock lithology is primarily composed of almond-shaped basalt and cryptocrystalline–microcrystalline basalt intercalated with brecciated lava. Among the layers, $P_2\beta_3^2$ and $P_2\beta_3^3$ are columnar jointed basalt layers. The rock flow layers are inclined with a strike trending $N40^\circ-50^\circ E$, $SE\angle 15^\circ-25^\circ$.

On the left bank, the spacing of the three diversion tunnels’ axes is 60.0 m. The tunnel cross-sections are arch-shaped measuring 17.5×22.0 m. The overlying rock mass in the No. 1 diversion tunnel has a thickness of 30–397 m and a horizontal depth reaching 705 m. The overlying rock mass

in the No. 2 diversion tunnel has a thickness of 50–380 m and a horizontal depth reaching 765 m; in the No. 3 diversion tunnel, the overlying rock mass has a thickness of 38–358 m and a horizontal depth reaching 825 m.

On the right bank, the spacing between them is also 60.0 m. The tunnel size is the same as on the left bank. The overlying rock mass in the No. 4 diversion tunnel has a thickness of 17–459 m and a horizontal depth reaching 290 m; in the No. 5 diversion tunnel, the overlying rock mass is found to have a thickness of 14–518 m and a horizontal depth reaching 360 m. The distribution of columnar jointed rock masses in diversion tunnel is shown in Table 1.

2.3 In situ Stresses

According to field hydraulic fracturing tests and the stress relief method, the major and minor principal stresses on the five diversion tunnels are shown in Fig. 6. Since the maximum difference in burial depth of the No. 1, No. 2, and No. 3 diversion tunnels is no more than 40 m, the same in situ stress at left bank is used for them. The No. 4 and No. 5 diversion tunnels are also similar. Therefore, different in situ stresses are adopted for the left and right bank. The intermediate principal stress on the left bank is

Fig. 4 Layout of the diversion tunnel at Baihetan Hydropower Station

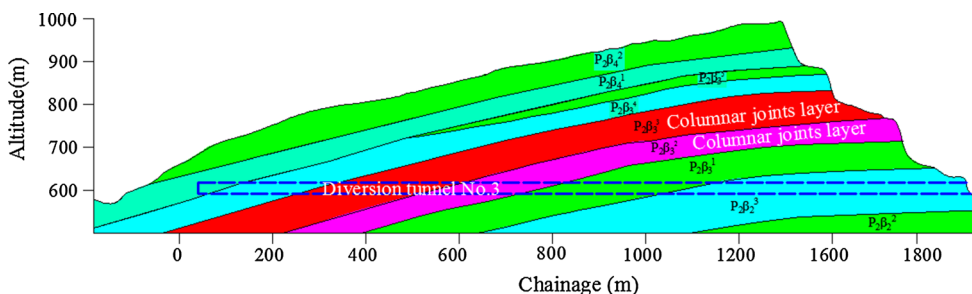
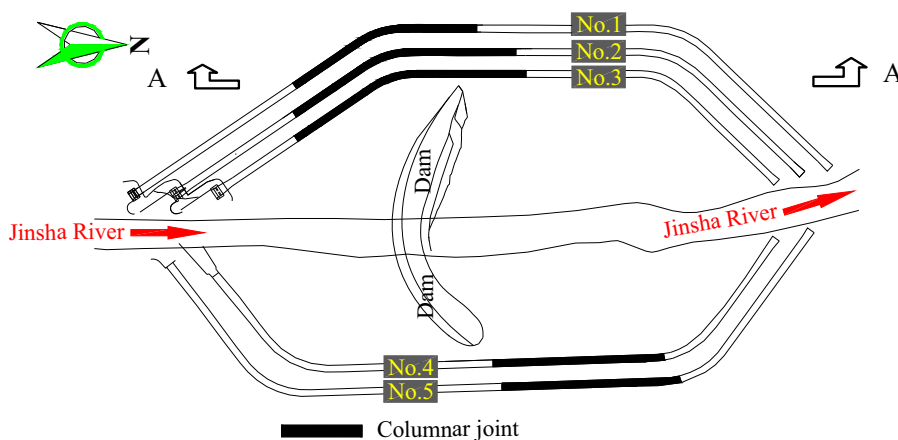
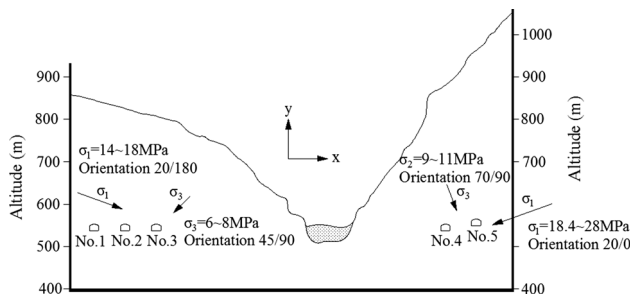


Fig. 5 Longitudinal geological section along the No. 3 diversion tunnel (section A–A in Fig. 4, in which $P_2\beta_3^2$ and $P_2\beta_3^3$ are columnar jointed basalt layers)

Table 1 Distribution of columnar jointed rock mass in diversion tunnel

Diversion tunnel no.	Tunnel length (m)	Columnar jointed rock mass			
		Chainage (km + m)	Chainage (km + m)	Length (m)	Percentage (%)
1	2009	0 + 400	0 + 870	470	23
2	1791	0 + 280	0 + 840	560	31
3	1587	0 + 250	0 + 710	460	29
4	1667	0 + 880	1 + 235	355	21
5	1946	1 + 070	1 + 510	440	23

**Fig. 6** In situ stress around the diversion tunnels at Baihetan hydropower station

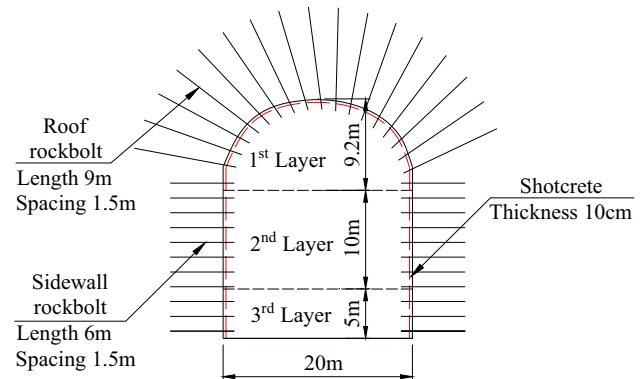
–9 to –12 MPa at an orientation of 35/45; while that on the right bank is –10 to –13 MPa at an orientation of 120/30. In addition, the axis of the diversion tunnel ran N/S. It is observed that the in situ stress on the right bank is higher than that on the left. Additionally, based on the different vertical depths of the five diversion tunnels, their geostatic stresses are calculated as 10.6, 10.6, 10, 12.8, and 14.5 MPa, respectively.

2.4 Excavation Method

The diversion tunnels are excavated in three layers, as shown in Fig. 7. The heights of the first, second, and third layers are 9.2, 10, and 5 m, respectively. Each layer is excavated by drilling and blasting, with smooth blasting adopted for the design contours. The blast circulating footage is approximately 3.0 m.

2.5 Support System

The support system for the diversion tunnel is predominantly ordinary grouted anchors, for which a 6 m anchor bolt is used for the sidewall, and a 9 m anchor bolt for the arch, with a bolt spacing of 1.5 m (Fig. 7). High-strength twisted steel bolts are used in the diversion tunnel. The outside diameter of the bolts is 32 mm. A hollow internal is used for the grouting. The maximum load capacity of the anchor is 50 kN/m. Before anchor bolt construction, steel

**Fig. 7** Typical support system for diversion tunnels

fibre reinforced concrete is sprayed on the exposed faces to form an initial support.

3 Evolution of EDZ in a Columnar Jointed Rock Mass with Field Measurement Data

3.1 Geometrical Features of the Columnar Joints

The columnar jointed basaltic rock masses exhibit regularly oriented prismatic structures, as shown in Fig. 1b. The primary cause of the columnar joints is tensile stress created by thermal contraction during cooling. The joint between columns commonly existing in the columnar joints is produced under tensile stress. The joint between columns is often found to form a hexagonal configuration due to sufficient condensation, such as in the Giant's Causeway in the UK, which is shown in Fig. 1a. While for the columnar joints at Baihetan, due to insufficient condensation, no regular columnar joints are formed. The columns are in trilateral, quadrangular, pentagonal, and hexagonal shapes, as shown in Fig. 8a, b. The joint between columns shows a rough granular surface, as shown in Figs. 9 and 10a. The column enclosed by this type of joint has a unilateral length of about 12 cm, a height of 2–3 m, and a dip angle of 75°–85°.

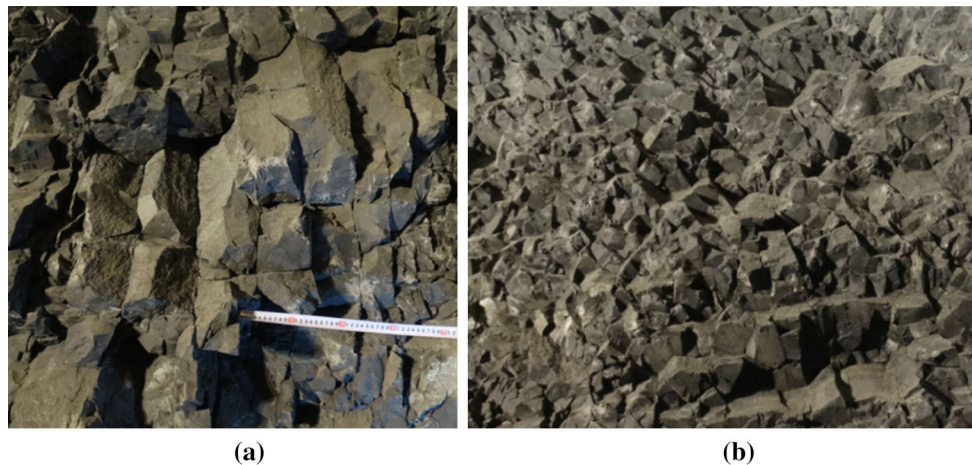


Fig. 8 Columnar joints at **a** sidewall of tunnel and **b** arch of tunnel

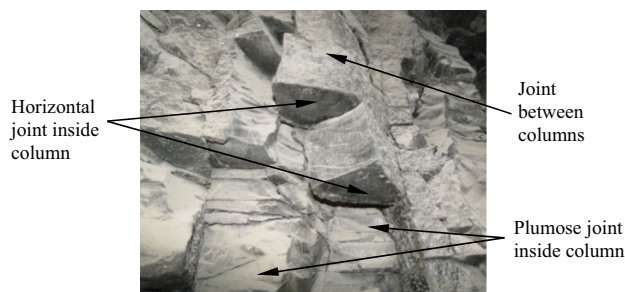


Fig. 9 Different types of joint planes in columnar joints

Further field surveys demonstrate that the joint planes within a columnar joint in the diversion tunnel are found to not only contain joint between columns, but also joints inside column as shown in Fig. 9. The joints inside column are interacting with each other and exhibiting a high strength before excavation, however, the strength is reduced after excavation because joint opening and slip-ping would occur in the joints inside a column.

The joints inside each column mainly include two types: plumose joint with a steep angle and horizontal (or near-horizontal) joints (James and Atilla 1987). The plumose joint has an undulating surface with a general wavelength of about 10 cm and a spacing of approximately 1.5–7.5 cm (Fig. 10b). The horizontal joints are often flat with a smaller spacing of 1–6 cm, and a length of about 25–100 cm (Fig. 10c). These three joint planes are intersecting thereby resulting in the columnar joint collapsing easily.

3.2 Micro-Fracture Pattern of Columnar Joints

During rock fracturing, the micro-morphology of the fracture surface is determined from its failure mechanisms such as shear or tensile failure (Cruikshank 1996; Kruhl

2013; Martin et al. 2014). Therefore, the fracture pattern of rock could be deduced by examining the micro-morphology of the fracture surface (Kuzmin and Skibitskaya 2011; Erarslan and Williams 2013). To obtain the characteristics of the fracture surface at a microscopic level, SEM imaging was used in this study as elsewhere (Belin 1992; Krinsley et al. 1998). The fracture surfaces of every joint plane collected in situ are directly examined by SEM in this study, without preparation of thin sections to avoid creating extra micro-cracks during preparation. The rock samples are collected from a collapsed section (chainage of K1 + 150 in the No. 5 diversion tunnel) which has been excavated over a long period to ensure that the failure of the sample is induced by excavation, and not blasting.

The micro-structural features of the joint between columns are shown in Fig. 11. A dry land pattern is found in Fig. 11a, b. This is a typical pattern formed by tensile stress. For the joint between columns, this pattern is formed by the condensation of magma, demonstrating that this joint is the primary joint. In addition, the shear trace shown in Fig. 11c and tension trace shown in Fig. 11d induced by excavation are also found in the joint surface, indicating that part of the joint between columns underwent shear failure, while others underwent tensile failure.

The micro-structural features of plumose joint are shown in Fig. 12. The fracture surface undulates and has sharp edges, which are typical features of a tensile failure. The plumose joint mainly underwent tensile failure.

The micro-structural features of horizontal joints inside column are shown in Fig. 13. The results showed that the crystals are well developed and that there are no obvious tensile or shear failure features.

Taken together, the shear failure mainly occurs at joint between columns, and tensile failure mainly occurs at joint between columns and plumose joint.

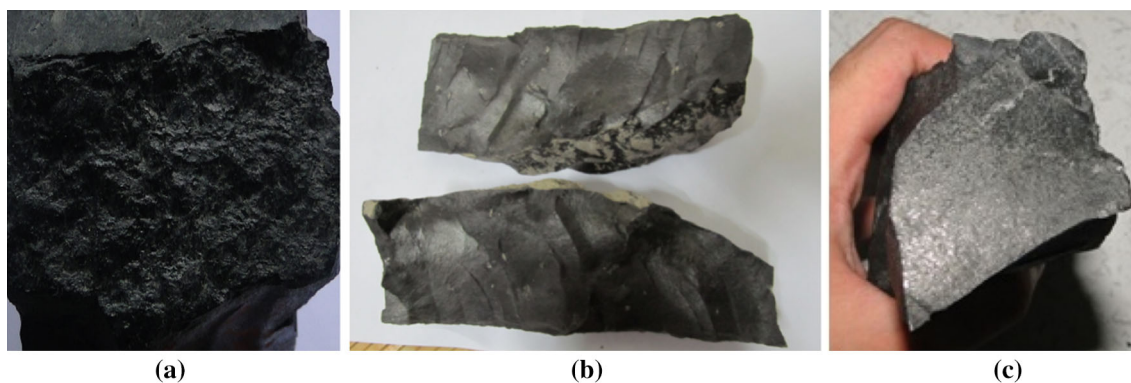


Fig. 10 Surface characteristics for **a** joint between columns, **b** plumose joint inside column and **c** horizontal joint inside column

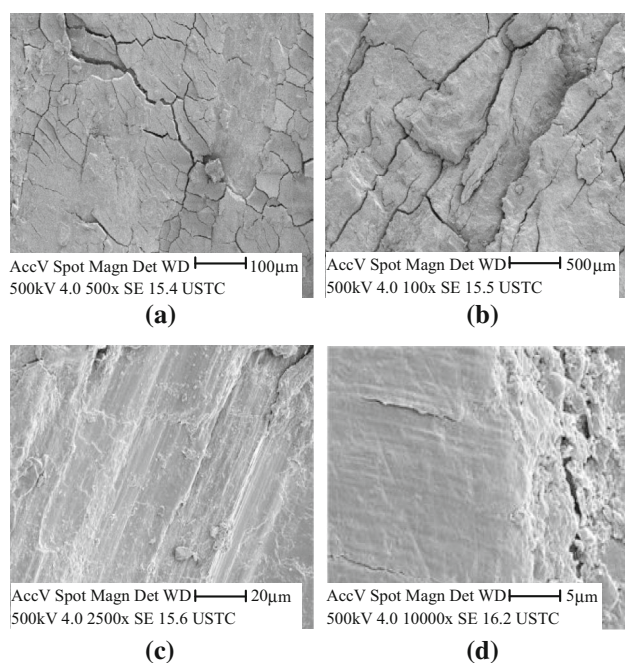


Fig. 11 Representative SEM patterns of joint between columns in **a** dry land pattern, **b** another dry land pattern, **c** parallel shear traces and **d** snake slide pattern with tear feature

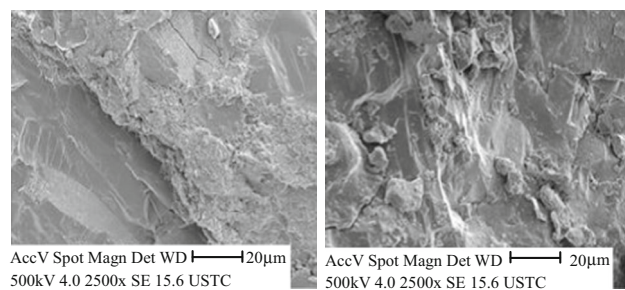


Fig. 12 Representative SEM patterns of plumose joint inside column

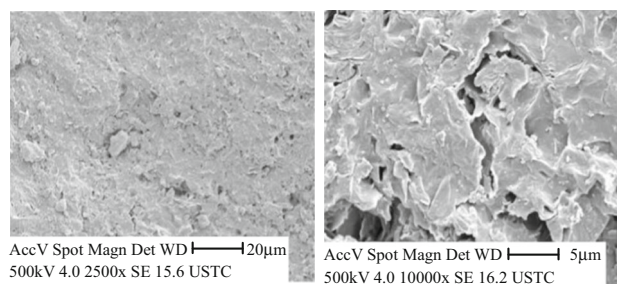


Fig. 13 Representative SEM patterns of horizontal joint inside column

3.3 Time-Dependent Crack Propagation and EDZ Development of Columnar Joints

3.3.1 Monitoring Equipment and Scheme

Several methods have been developed to characterize the depth of the EDZ, which include tunnel and borehole investigations (Mertens et al. 2004; Hudson et al. 2009; Shao et al. 2008). The latter contains occurrences of macroscopic fractures, borehole geophysics, and borehole hydraulic tests. Several borehole geophysical techniques are available for estimating the depth of an EDZ, e.g. P-wave velocity measurements and digital borehole camera inspection. In this study, digital borehole camera is used to monitor crack propagation, and P-wave velocity measurements along the boreholes are used to estimate the depth of the EDZ.

The distribution and development of cracking is significant for evaluating the stability of rock masses. Using a digital borehole camera, although the instruments are difficult to instal and only small areas can be observed, the fractures and their time-dependent development in the boreholes could be clearly, and directly, observed. The extent of EDZ and its development after excavation could be

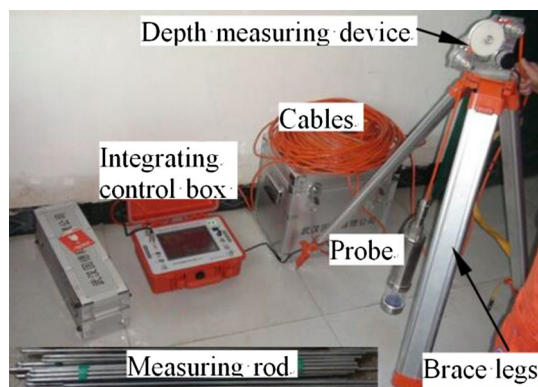


Fig. 14 Basic equipment for a typical borehole digital camera system

also obtained. The EDZ can be identified by directly observing fracture modifications exploiting the precision of the digital borehole camera (Wang et al. 2002; Li et al. 2012).

The equipment items for a typical borehole digital camera system are shown in Fig. 14.

The operating procedure for this borehole digital camera system is as follows:

1. Selection of the drilling position: for convenient measurement, the boreholes are within 2 m to the tunnel bottom. The boreholes are drilled before, or immediately after, the excavation to comprehensively obtain the development of any subsequent fractures.
2. Drilling and examination of the boreholes: percussive and rotary drilling methods are applied at a constant speed below 600 rpm. After being drilled, the boreholes should be washed out using clean water.
3. Fracture measurement: after connecting all the equipment, a probe is sent to the bottom of the borehole to record the fracture pattern of the borehole in video format. Images demonstrating the crack pattern in all directions are extracted using image capture software.
4. Calculation of fracture width: it is calculated by measuring the distance between two points on the edges of a fracture in the captured images.
5. Fracture development: this is obtained by measuring the width of a fracture in the same borehole at different times.

The construction of the diversion tunnels began in April 2012, and the excavation was completed by June 2013. The depth of the EDZ of the columnar joints at several sections was monitored during construction, including: chainage K0 + 315 and K0 + 325 in the No. 0.3 diversion tunnel; chainage K1 + 040 and K1 + 050 in the No. 4 diversion tunnel; and chainage K1 + 050 in the No. 5 diversion tunnel. The disposition of the boreholes used for digital borehole camera and acoustic wave measurements at these monitoring sections is shown in Fig. 15. In total, the wave velocity at different time of ten boreholes was monitored.

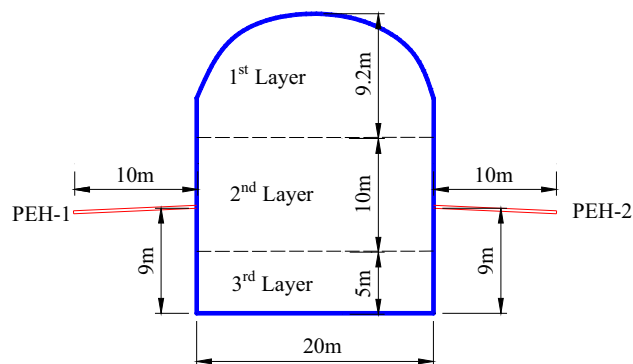


Fig. 15 Layout of drilled boreholes for ultrasonic P-wave velocity tests and digital borehole camera inspection (taking chainage K1 + 040 at No. 4 diversion tunnel as an example)

The intelligent acoustic instrument RSM-SY5 developed by the Institute of Rock and Soil Mechanics, Chinese Academy of Science, is used here. At the test site, a single borehole transducer is placed on the bottom of a borehole and a bottom-up approach is used.

3.3.2 Determination Methods of EDZ

The extent of the EDZ is determined by ultrasonic velocity test and digital borehole camera. For the ultrasonic velocity test, the EDZ could be defined as the zone with a low wave velocity. Considering digital borehole camera images, the EDZ in the rock mass is identified on the basis of new fractures observable via the precision of the digital optical borehole camera. As demonstrated in Fig. 16, the zone with lower P-wave velocities shows well-developed cracking, while the zone with higher P-wave velocities has relatively intact rock masses. The measured ultrasonic velocity data and digital borehole camera images agreed well with each other, which verified that the combination of these two methods is effective in measuring the extent of the EDZ.

3.3.3 Monitoring Results of Crack Propagation

The evolutionary characteristics of the crack propagation in columnar jointed rock masses are observed by a digital borehole camera at a resolution of 0.2 mm (Wang et al. 2002; Li et al. 2012). A series of colour digital images reveal the process of crack propagation as shown in Fig. 17.

As shown in Fig. 17, the cracks observed in the columnar jointed rock mass have significant time-dependent behaviour. Take borehole PEH-1 at chainage K1 + 040 shown in Fig. 17a as an example, this section was excavated on 8 January, 2013. Several cracks are observed in this borehole after excavation. Within 10 days

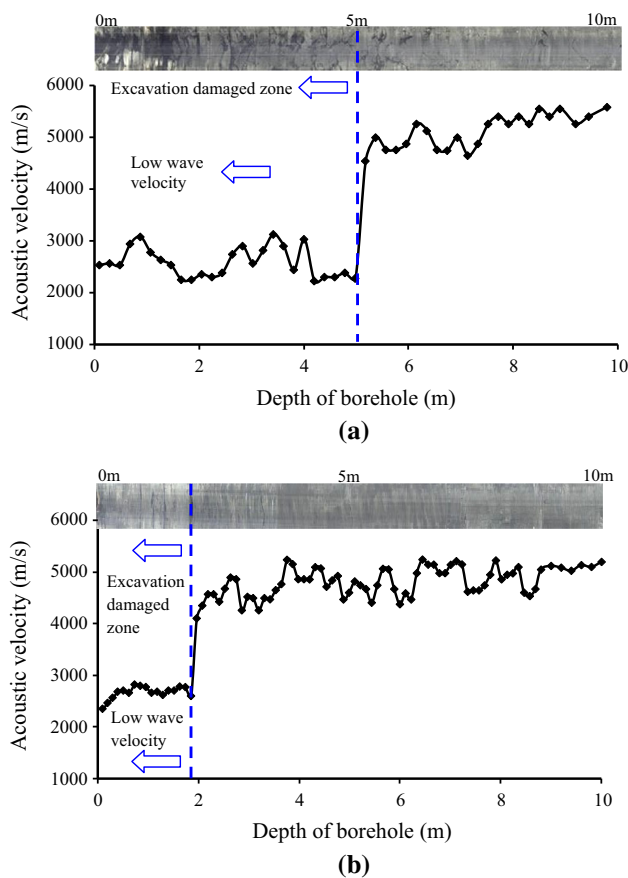


Fig. 16 Measuring method of EDZ by the relationship between borehole wave velocity, crack development and the depth away from the tunnel wall at **a** chainage K1 + 050, No. 4 diversion tunnel and **b** chainage K0 + 315, No. 3 diversion tunnel, right bank

after excavation, the cracks are enlarged under the influence of the face advance. After 10 days' excavation, the tunnel face was 40 m from the monitoring section, which was greater than two times the tunnel diameter. After this time, the crack propagation was not influenced any further by the face advance. However, after 43 and 49 days of excavation, the cracks are still growing. The maximum extension of any single crack was up to 9.8 mm at this time. This demonstrates that the crack lengths increased with time, even if the tunnel face did not affect them any further. Crack propagation in a columnar jointed rock mass exhibits significant time-dependent behaviour. The analysis of Fig. 17b follows the analysis outlined above.

However, the strength of the rock mass is not decreased until the cracking developed to a certain extent. As this extent has not yet been elucidated thoroughly, and this research focused on the development of collapse, an equivalent concept is applied. The rock masses would damage gradually and would finally collapse if there are no control devices present as the cracking, or joints, opened and developed. Based thereon, the strength of the columnar

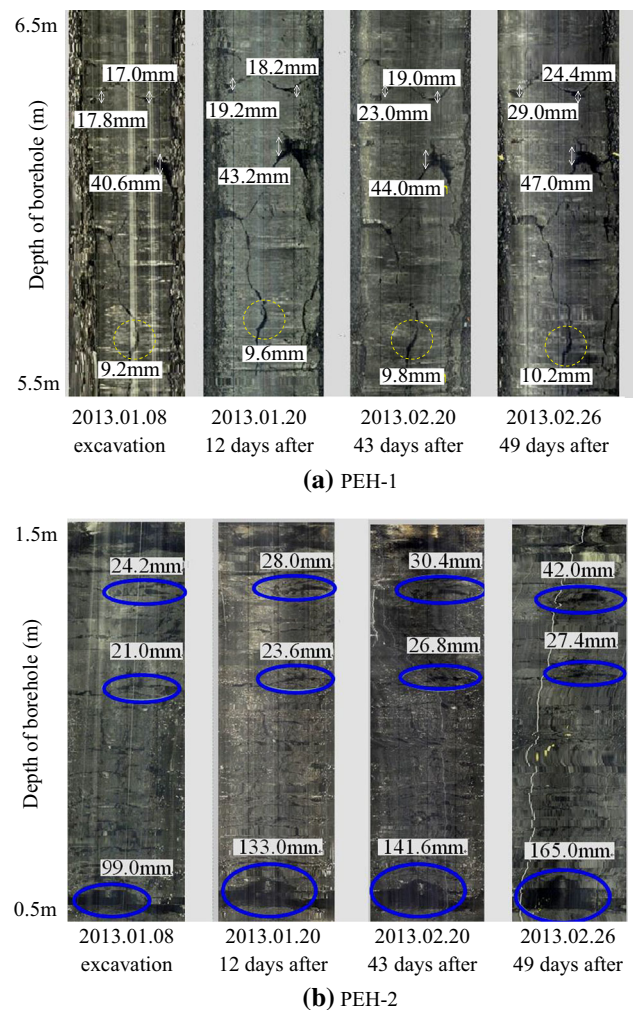


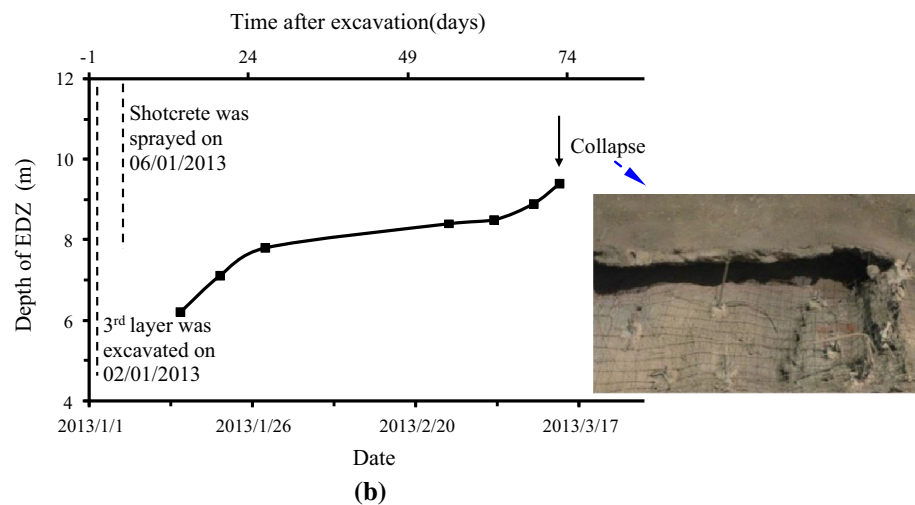
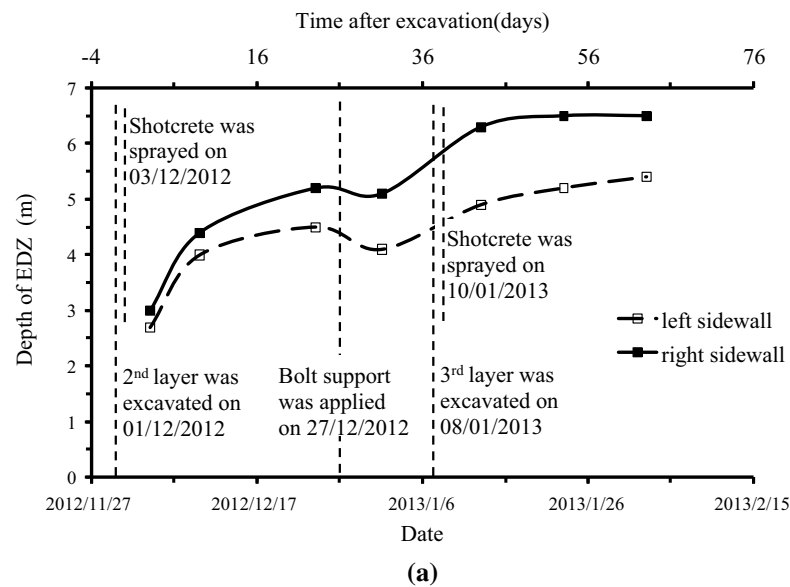
Fig. 17 Crack propagation in borehole **a** PEH-1 at depths of 5.5–6.6 m and **b** PEH-2 at depths of 0.5–1.5 m shown in flat wall images at different times, including the day of excavation, 12 days post-excavation, 43 days post-excavation and 49 days post-excavation

jointed rock mass decreased with increasing cracking; if the continuous development of cracking is not inhibited, collapse would occur.

3.3.4 Monitoring Results of Time-Dependent EDZ Development

After excavation of the monitored sections, the depth of the EDZ at each position is measured at least once every 10 days. The EDZ development over a lengthy period of time is monitored, combined with its relationship with the excavation and support. This study focused on the chainage K1 + 040 in the No. 4 diversion tunnel and chainage K1 + 050 in the No. 5 diversion tunnel to illustrate the variations of the EDZ evolution of the columnar jointed rock mass.

Fig. 18 EDZ development after excavation at **a** chainage K1 + 040 of No. 4 diversion tunnel and **b** chainage K1 + 050 of No. 5 diversion tunnel at right bank



As shown in the Fig. 18a, the second layer at chainage K1 + 040 was excavated on 1 December, 2012. After 3 days, the depth of the EDZ has increased to 2–3 m and it then reached 3.8–4.2 m 10 days later. At this point, the tunnel face was approximately 40 m past this monitoring station, and the excavation of the tunnel face did not have any influence on the EDZ development of this monitoring station any more. After 23 days, the depth of the EDZ still continued to increase by up to 4–5 m. This indicates obvious time-dependence behaviour of such columnar jointed rock masses. After 26 days, support was installed, after which the depth of the EDZ decreased demonstrating that support could restrain the deformation and cracking evolution of columnar joints. Subsequently, under the influence of the third layer of excavation, the depth of the EDZ increased again. After 10 days of the completion of excavation, the depth of the EDZ continued to increase. It is shown that the EDZ of the supported columnar jointed rock mass is still

time-dependent, but its development slowed compared to that seen in unsupported cases. The rate of increase of the depth of the EDZ at chainage K1 + 040 began quickly, and then tapered off. The depth of the EDZ at this monitoring station only experienced a deceleration stage.

However, the depth of the EDZ at chainage K1 + 050 in the No. 5 diversion tunnel on the right bank experienced all three stages of EDZ development, as shown in Fig. 18b. The third layer at this station was excavated on 2 January, 2013, and from then on the depth of the EDZ constantly increased, but the rate of increase decreased. At this time, the evolution of the EDZ was in its deceleration stage. After a month of excavation, the rate of increase of the depth of the EDZ was stable and it entered its stabilization stage. Along with the development of the EDZ, due to the support not being installed, the depth of the EDZ experienced a sudden rapid growth after two months of excavation. The corresponding rate of increase of EDZ depth was also increasing, indicating

that it had entered its acceleration stage. After a further 20 days at this stage, collapse occurred to a failure in the columnar jointed rock mass. The collapse mainly occurred in the sidewall at chainage K1 + 150 to K1 + 165 with a collapse area of 15 m × 10 m and a depth of 2 m. Some 15 days post-collapse, the zone was reinforced mainly using pre-stressed anchor bolts and wire mesh. The zone was thus finally stabilized.

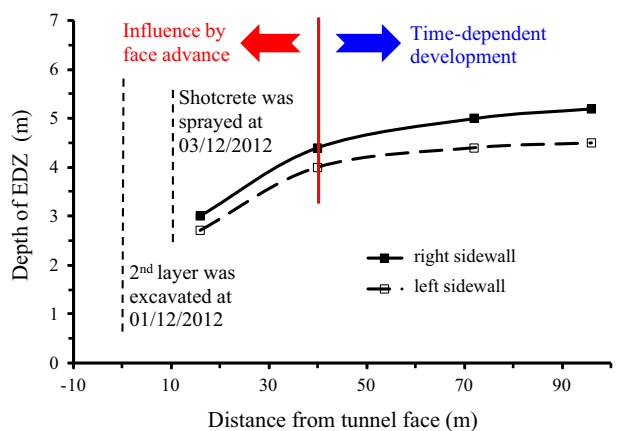
Through the analysis of the development of the EDZ at the aforementioned monitoring station, it is shown that when the tunnel face has passed the monitoring station by about 40 m or so (two times the tunnel diameter, which requires about 10 days of excavation), the excavation of the tunnel face no longer exerted any influence on the monitoring station (Fig. 19). However, the depth of the EDZ still increased given the time-dependent behaviour of the columnar joints. Even after the tunnel has been supported, the depth of the EDZ is still time-dependent and increasing. The trend certainly slowed a great deal compared with that in unsupported cases. Similar to a creep curve, the time-dependent EDZ development curve also generally includes three stages (see Fig. 20): (1) the deceleration stage, which the jointed rock mass must experience. In this stage, the initial rate of increase of the depth of the EDZ is rapid, but it then decreases with time; (2) the stabilization stage, in which the rate of increase of the depth of the EDZ is relatively uniform; and (3) the acceleration stage, in which the rate of increase of the depth of the EDZ increases sharply, which leads to the instability of the rock mass and its ultimate failure.

As shown above, the time-dependent crack propagation in the columnar jointed rock mass leads to the increase of the depth of EDZ and decrease of the strength of the columnar jointed rock mass. The characteristic of time-dependent EDZ evolution is remarkable. However, the creep behaviour of the columnar jointed rock mass is not significant as shown in Fig. 21. The long-term stability of columnar jointed rock mass is primarily reflected on the time-dependent crack propagation, and not on the creep. Therefore, the creep model could not be used here. A time-dependent strength model for columnar joints needs to be proposed to solve the problem of the time-dependent development of EDZ in columnar jointed rock mass.

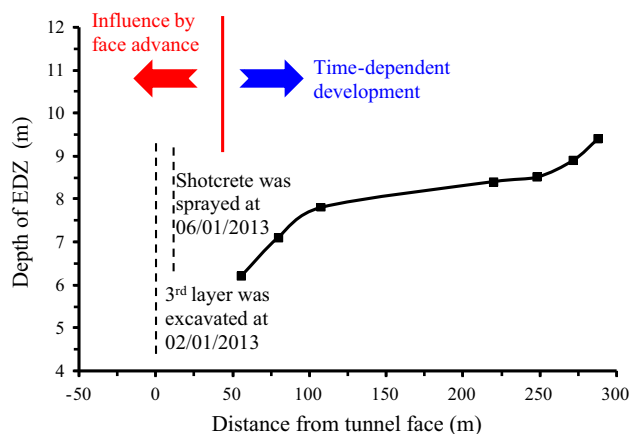
4 Time-Dependent Strength Model for a Columnar Jointed Rock Mass

4.1 Deformation Behaviour

For multiple joint planes, the local coordinate system is independently established for each set of joint planes. The orientations are expressed by the joint plane dip dip^{ji} and



(a)



(b)

Fig. 19 EDZ development due to face advance and time dependency at **a** chainage K1 + 040 of No. 4 diversion tunnel and **b** chainage K1 + 050 of No. 5 diversion tunnel at right bank

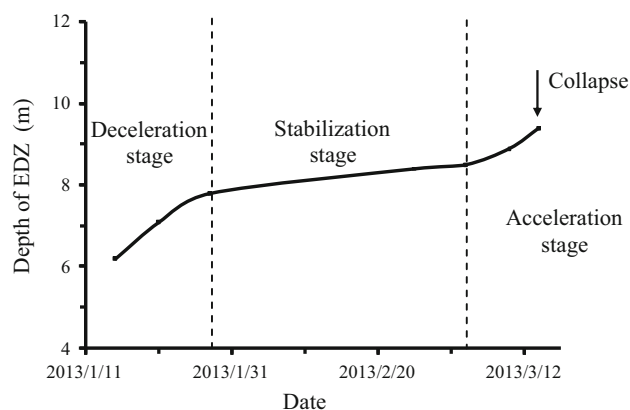


Fig. 20 Complete time-dependent evolution curve of the depth of the EDZ for the columnar jointed rock mass

azimuth dd^{ji} , respectively, where super- or subscript ji represent the i th set of joint planes. As three types of joints are found in the columnar jointed rock mass, the

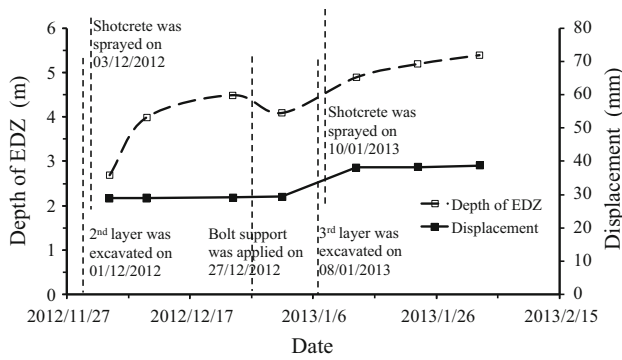


Fig. 21 Time-dependent EDZ and displacement evolution at chainage K1 + 040 of No. 4 diversion tunnel at right bank

superscripts or subscripts j_1, j_2, j_3 represent the joint between columns, plumose joint inside a column, and horizontal joint inside a column, respectively.

The elastic behaviour of a rock mass containing multiple joints includes the elastic deformation of both intact rock and joints, as follows:

$$d\varepsilon = d\varepsilon^I + d\varepsilon^J \tag{1}$$

where $d\varepsilon, d\varepsilon^I,$ and $d\varepsilon^J$ represent the strain increment of the jointed rock mass, intact rock, and the joints, respectively.

$$d\sigma = [K]d\varepsilon^I \tag{2}$$

where $d\sigma$ is the stress increment and $[K]$ is the global stiffness matrix. Considering the highly transverse characteristics of columnar jointed rock mass (King et al. 1986; Jiang et al. 2014), the transverse stiffness matrix is selected to represent this anisotropic feature. Its detailed component is as below:

$$[K] = \begin{bmatrix} C_{11} & C_{12} & C_{13} & 0 & 0 & 0 \\ C_{12} & C_{22} & C_{13} & 0 & 0 & 0 \\ C_{13} & C_{13} & C_{33} & 0 & 0 & 0 \\ 0 & 0 & 0 & C_{44} & 0 & 0 \\ 0 & 0 & 0 & 0 & C_{66} & 0 \\ 0 & 0 & 0 & 0 & 0 & C_{66} \end{bmatrix} \tag{3}$$

where,

$$C_{11} = C_{22} = \frac{E_1(1-n\mu_{13}^2)}{(1+\mu_{12})(1-\mu_{12}-2n\mu_{13}^2)}, \quad C_{12} = \frac{E_1(\mu_{12}+n\mu_{13}^2)}{(1+\mu_{12})(1-\mu_{12}-2n\mu_{13}^2)},$$

$$C_{13} = \frac{E_1\mu_{13}}{1-\mu_{12}-2n\mu_{13}^2}, \quad C_{33} = \frac{E_3(1-\mu_{12})}{1-\mu_{12}-2n\mu_{13}^2}, \quad C_{44} = \frac{E_1}{1+\mu_{12}},$$

$$C_{66} = 2G_{13}, \quad n = \frac{E_1}{E_3}.$$

In which, E_1, μ_{12} is the elastic modulus and Poisson’s ratio at the isotropic direction, respectively, and E_3, μ_{13}, G_{13} is the elastic modulus, Poisson’s ratio and shear modulus at the anisotropic direction, respectively.

For elastic deformation of the joints, a representative unit volume containing n joint sets is considered. The unit stress under a global coordinate system is converted into a joint stress field under a local coordinate system through

the use of a coordinate transformation matrix. The relationship between the joint stress and strain is then established as follows:

$$d\sigma = [R^{ji}][K][R^{ji}]^T d\varepsilon^{ji} \tag{4}$$

where $d\varepsilon^{ji}$ is the elastic deformation of the i th set of joint planes, $[R^{ji}]$ is the transformation matrix of the i th set of joint planes, which is closely related to the dip and inclination of the joint plane (Singh et al. 2002). The transformation matrix is used to convert the global coordinate system to the local coordinate system of joint. The transformation matrix constitutes the direction cosines $[l_i, m_i$ and n_i ($i = 1, 2, 3$)] of unit vector of local coordinate system of joint (x', y', z') on the global coordinate system (x, y, z) . Its expression is as:

$$[R] = \begin{bmatrix} l_1^2 & m_1^2 & n_1^2 & 2m_1n_1 & 2n_1l_1 & 2l_1m_1 \\ l_2^2 & m_2^2 & n_2^2 & 2m_2n_2 & 2n_2l_2 & 2l_2m_2 \\ l_3^2 & m_3^2 & n_3^2 & 2m_3n_3 & 2n_3l_3 & 2l_3m_3 \\ l_2l_3 & m_2m_3 & n_2n_3 & R_{44} & R_{45} & R_{46} \\ l_3l_1 & m_3m_1 & n_3n_1 & R_{54} & R_{55} & R_{56} \\ l_2l_1 & m_2m_1 & n_2n_1 & R_{64} & R_{65} & R_{66} \end{bmatrix} \tag{5}$$

where

$$R_{44} = m_2n_3 + m_3n_2, R_{45} = n_2l_3 + n_3l_2, R_{46} = l_2m_3 + l_3m_2, R_{54} = m_3n_1 + m_1n_3, R_{55} = n_3l_1 + n_1l_3, R_{56} = l_3m_1 + l_1m_3$$

$$R_{64} = m_1n_2 + m_2n_1, R_{65} = n_1l_2 + n_2l_1, R_{66} = l_1m_2 + l_2m_1, l_1 = \sin(dd) \cos(dip), m_1 = \cos(dd) \cos(dip)$$

$$n_1 = -\sin(dip), l_2 = -\cos(dd), m_2 = \sin(dd), n_2 = 0, l_3 = \sin(dd) \sin(dip), m_3 = \cos(dd) \sin(dip), n_3 = \cos(dip)$$

where dip is short for the dip angle and dd is short for the dip direction. The different dip and dip direction of joint corresponding to different $[R^{ji}]$.

As the deformation of all joints is the sum of the deformation of each set of joint planes, the deformation of all joints is as follows:

$$d\varepsilon^J = \sum_{i=1}^n d\varepsilon^{ji} \tag{6}$$

4.2 Strength Criterion

Three types of joints are found in the columnar jointed rock mass, thus its failure modes are complex. They mainly include tensile and shear failure of the intact rock and joint planes, as well as their composite failure. The Mohr–Coulomb yield criterion with a tension cut-off limit is used to describe the intact rock. For the joint plane, these three

sets of joint planes have different surface roughness, thus different yield criteria are used as follows:

1. The surface of the joint between columns is granular and rough as shown in Fig. 10a. For the joints with a naturally rough surface, the rate of increase of shear strength decreased in the presence of a protrusion which is gradually sheared by the increasing normal stress, which leads to the non-linear relationship between joint shear strength and normal stress. Thus, the Barton–Bandis joint criterion with a tension cut-off limit is used.
2. The plumose joint inside column has a parallel structure with a spacing of 10 cm as shown in Fig. 10b. The depth of the plumose structure is approximately 2 cm, therefore the joint surface is very rough and the Barton–Bandis joint criterion with a tension cut-off limit is used.
3. The surface of the horizontal joints inside the column is flat with a near-horizontal direction as shown in Fig. 10c. It is deemed better to use the Mohr–Coulomb criterion with a tension cut-off limit to describe this smooth joint plane.

For the horizontal joints inside a column, the shear yield criterion, tensile yield criterion, and shear-tensile boundary mixed criterion, respectively, are as follows: $f_{j3}^s = \tau_{j3} - \sigma_{3'3'} \tan \phi_{j3} - C_{j3}$ for the shear criterion of horizontal joints inside a column $f_{j3}^t = \sigma_{3'3'} - \sigma_{j3}^t$ for the tension criterion of horizontal joints inside a column $h_{j3} = \tau_{j3} + \sigma_{j3}^t \tan \phi_{j3} - C_{j3} + (\sqrt{1 + \tan^2 \phi_{j3}} - \tan \phi_{j3})$ for the shear-tension boundary mixed criterion of horizontal joints inside a column where f_{j3}^s , f_{j3}^t , and h_{j3} are the shear, tension, and shear-tensile boundary mixed criteria for the horizontal joint inside a column, respectively; τ_{j3} , and $\sigma_{3'3'}$ are the shear stress and normal stress on the horizontal joint inside a column; C_{j3} , ϕ_{j3} , and σ_{j3}^t are the cohesion, friction angle, and tensile strength of the horizontal joint inside a column.

With regard to the joints between a column and a plumose joint, their tensile yield criteria are the same as those horizontal joints within columns. Their shear yield criterion is as follows (Barton 1976):

$$f_{ji}^s = \tau_{ji} - \sigma_{3'3'}^i \tan \phi_m^i$$

$$\phi_m^i = \text{JRC}^{ji} \lg \left(\frac{\text{JCS}^{ji}}{|\sigma_{3'3'}^i|} \right) + \phi_r^i \quad (7)$$

where f_{ji}^s , ϕ_m^i , ϕ_r^i , JRC^{ji} , and JCS^{ji} are the shear criterion, friction angle considering dilatancy effects, residual friction angle, joint roughness coefficient, and joint wall compressive strength of the i th set of joint planes,

respectively ($i = 1$, joint between columns; $i = 2$, plumose joint inside a column).

For the shear-tension boundary mixed criterion of joints between a column and a plumose joint:

$$h_j^B = \tau_{ji} - \sigma_{3'3'}^i \tan \phi_m^i + b_j^i \times (\sigma_{3'3'}^i - \sigma_j^{t,i}) \quad (8)$$

$$b_j^i = \frac{1}{264} \times \frac{\text{JRC}^{ji}}{\text{JCS}^{ji}} \quad (9)$$

where h_j^B is the diagonal line of Barton criterion of f_s and f_t and it is used to distinguish the shear and tensile failure zones.

In this program, when the rock mass showed elastic deformation, the stress increment is directly calculated through the elastic stress–strain relationship; for plastic deformation, the stress increment is determined by the plastic part of the total strain increment. Therefore, in the fast Lagrangian algorithm, the stress increments of rock and joints have to be modified, respectively, to obtain new stress increments and the updated stress state.

4.3 Time-Dependent Degradation Strength Model

According to the description in Sect. 3.3, the crack propagation and the depth of EDZ in a columnar jointed rock mass increased over time, suggesting that the strength of the joints exhibited time-dependent degradation after excavation.

After tunnel excavation, joints opening and slippage occur in the joints of the columnar jointed rock mass. These joint planes are compact before excavation, which leads to the high strength of the columnar joints. However, after excavation, cracks occurred in the joints, reducing the degree of compactness thereof. This process is equivalent to the reduction of the joint roughness coefficient (Zhao 1997). Moreover, with the passage of time, the extent of the cracking increases, leading to the roughness coefficient continuing to decrease, so that the joint roughness coefficient (JRC) shows a time-dependent decrease.

In addition, for the surrounding rocks, the excavation is a process changing the stress state from one entailing a high confining pressure to one with a low confining pressure. In the case of a high confining pressure, the basic friction angle ϕ_b of the joints plays a major role. In the case of a low confining pressure, combined with weathered joints due to the sidewall of the tunnel being exposed to atmosphere, the residual friction angle ϕ_r of the joints played a leading role (Yoshida and Horii 1992; Sellers and Klerck 2000; Kaiser and Kim 2015). Therefore, during excavation, the joint friction angle is weakened from the basic friction angle to a residual friction angle, and this process is time-dependent. In conclusion, the roughness

coefficient and friction angle of joints in the Barton–Bandis strength criterion showed a time-dependent characteristic after excavation. Furthermore, the depth of the EDZ in the supported rock mass is also shown to be time-dependent as described in Sect. 3.3.4. This indicates that the supported rock mass also underwent a time-dependent degradation of its mechanical properties, but the trend slowed a great deal in comparison to the unsupported case. Therefore, support must be considered in the time-dependent model. Not only that, according to the analysis in Sect. 3.3.4, when the tunnel strain ε in a columnar jointed rock mass has reached threshold values of ε_s and ε_a , it entered a stabilization stage and an acceleration stage, respectively. The time-dependent degradation coefficients are different at each stage. The strength of the rock mass is plotted in logarithmic, linear, and exponential forms over time in the deceleration, stabilization, and acceleration stage, respectively. Therefore, the time-dependent degradation coefficients of the columnar joints can be summarized as follows:

In the deceleration stage ($\varepsilon < \varepsilon_s$):

$$K_{JRC}/K_{\phi_r} = a \ln t + b \text{ joints can be summarised as} \quad (10)$$

$$K_{JRC}/K_{\phi_r} = c \ln t + d \text{ for the supported surrounding rock mass} \quad (11)$$

In the stabilization stage ($\varepsilon_a > \varepsilon \geq \varepsilon_s$):

$$K_{JRC}/K_{\phi_r} = gt + h \text{ for the unsupported surrounding rock mass} \quad (12)$$

In the acceleration stage ($\varepsilon \geq \varepsilon_a$):

$$K_{JRC}/K_{\phi_r} = ke^{ft} \text{ for the unsupported surrounding rock mass} \quad (13)$$

where K_{JRC} , K_{ϕ_r} are the time-dependent degradation coefficients of roughness coefficient and friction angle of the joints in the columnar jointed rock mass; a , b , c , d , g , h , k , and f are coefficients, which reflect the decreasing rate of strength with time.

5 Determination of Time-Dependent Degradation Coefficient of a Columnar Jointed Rock Mass by Back-Analysis

It can be seen from the above constitutive model that three sets of joints are found in the columnar jointed rock mass, leading to many parameters being required, and the parameter values being difficult to determine. Therefore, an intelligent back-analysis method is used to determine the unknown time-dependent coefficients of the constitutive model, such as a , b , c , or d in Eqs. (11–14).

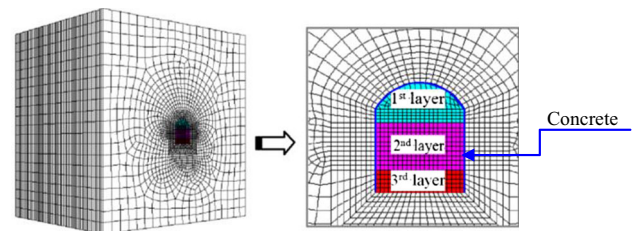


Fig. 22 Three-dimensional numerical simulation model of diversion tunnel

Table 2 Properties of the supporting materials

	E (MPa)	ν	σ_r (MPa)
Concrete	2.1×10^4	0.25	2.39
Rock bolt	20×10^4	0.20	440

5.1 Numerical Model

The three-dimensional numerical simulation model, as shown in Fig. 22, is excavated in three layers, and the height of each layer is shown in Fig. 15. The length of the model is 160 m, with square boundaries to minimize the influence of the boundary effect. The height and width of the model are both 200 m. The applied geo-stress is shown in Sect. 2.3. The constitutive model of the columnar jointed rock mass is described in Sect. 4. As the depth of the EDZ is affected by the grid size, mesh refinement within two times the tunnel diameter is used for increasing the precision and speed of the operation. A 1 m grid size, which is much smaller than the depth of the EDZ, is used. The support system of the columnar jointed rock mass consisted of grouted rock bolts and a 10 cm thickness of concrete (Fig. 7) which is installed after each excavation sequence. The concrete is usually sprayed after 2 days of excavation and the rock bolts are installed a month or more later. The properties of both rock bolts and concrete are shown in Table 2.

5.2 Determination of Time-Dependent Degradation Coefficient

The columnar jointed rock masses exhibited time-dependent EDZ evolution, demonstrating the fact that the depth of the EDZ is continually increasing, i.e. the mechanical parameters of the columnar jointed rock mass are constantly weakening. If the mechanical parameters at different times could be obtained by back-analysis of the depth of the EDZ at these times, then the variation of the mechanical parameters of a columnar jointed rock mass over time could be obtained. Finally, curve fitting is carried out to obtain the time-dependent coefficient of the columnar jointed rock mass.

It is observed from Fig. 17 that the depth of EDZ increased with time at different rates in different stages (the deceleration stage, the stabilization stage and the acceleration stage). In addition, it can be seen from Fig. 18 that the depth of EDZ decreased slightly after applying rock-bolt anchors and the rate of increase of the EDZ also decreased thereafter. Therefore, the time-dependent coefficient is closely related to the EDZ development stage and support system, thus various time-dependent coefficients for each EDZ development stage and support system are analysed.

5.2.1 Time-Dependent Coefficients Of Unsupported Columnar Joints in the Deceleration Stage

First of all, the time-dependent degradation coefficients of unsupported columnar joints in deceleration stage are calculated, i.e. *a* and *b* in Eq. (11) are solved. The data at Fig. 15 from 10 December to 27 December, 2012 at Chainage K1 + 040 in the No. 4 diversion tunnel are selected for back-analysis, during which the columnar jointed rock mass is unsupported.

It is well known that the rock properties measured in laboratory tests cannot be extrapolated directly to field scale. Therefore, it is essential to compare numerical simulations with measurements obtained from long-term monitoring of such tunnels to acquire the time-dependent degradation coefficients.

To date, back analyses have been helpful in obtaining the mechanical properties to analyse the time-dependent behaviour of tunnels. For example, Boidy et al. (2002) presented a back-analysis of the time-dependent behaviour of a monitored tunnel in Switzerland. Nadimi et al. (2011) presented a back-analysis of the time-dependent behaviour of the Siah Bisheh cavern using the 3D discrete element method. Mostafa et al. (2013) studied the long-term behaviour of a tunnel lining by numerical simulation, in which the properties of the model are obtained by back-analysis. Therefore, the back-analysis method has been used to obtain the unknown parameters for the time-dependent constitutive modelling of columnar joints.

According to the intelligent back-analysis method (Feng et al. 2006), the following elements are required:

1. In situ monitoring data, which are introduced in Sect. 3.
2. A representative calculation model, which included the constitutive model and grid model, in which, the constitutive model considering time-dependent evolution of the EDZ is introduced in Sect. 4; the grid model is described in Sect. 5.1.
3. The parameters which need to be back-analysed. This could be achieved by sensitivity analysis. The sensitivity analysis method adopted in this study is the same as that proposed by Mostafa et al. (2013). The results show that the residual friction angle ϕ_r^{j1} and the roughness coefficient JRC^{j1} of joint between columns significantly influenced the stability of columnar joints, whereas the tensile strength of the joint between columns and plumose joint are less important. The other parameters have little influence on the stability of the columnar joints. This demonstrates that the depth of the EDZ in a columnar jointed rock mass is mainly related to the shear properties of the joint between columns.
4. The parameters that could be directly obtained from laboratory and in situ testing (Zhang et al. 2011) are listed in Table 3, where E_1 , E_2 , ν_1 , and ν_2 are the elastic moduli and Poisson's ratio of the basalt perpendicular and parallel to the column axis; G , C_0 , ϕ_0 , and σ_t are the shear modulus, cohesion, friction angle, and tensile strength of the basalt.
5. A certain amount of computing scheme and corresponding results, in which the scheme is obtained by uniform design.
6. An efficient algorithm that reduced the error between the measured and calculated EDZ. In this research, artificial neural networks and a genetic algorithm are used (Feng and Hudson 2009).

There are four parameter levels of JRC^{j1} and ϕ_r^{j1} , i.e. (5, 7, 9, and 11) and (16, 20, 24, and 28), which are used for uniform design. A total of 16 sample schemes are designed. The depth of the EDZ both at the right and left sidewalls is obtained by substituting these samples into the numerical simulation model. These 16 data sets are divided randomly into two data sets. The first data set containing 12 data sets is used in training the artificial neural networks to obtain

Table 3 Directly obtainable parameters

Rock mass parameters	E_1 (GPa)	E_2 (GPa)	ν_1	ν_2	G (GPa)	C_0 (MPa)	ϕ_0 (°)	σ_t (MPa)	
Values	10.5	8.6	0.26	0.26	8.63	6	37	1.5	
Joint parameters	JCS^{j1} (MPa)	σ_t^{j1} (MPa)	ϕ_r^{j2} (°)	JRC^{j2}	JCS^{j2} (MPa)	σ_t^{j2} (MPa)	C_{j3} (MPa)	ϕ_{j3} (°)	σ_t^{j3} (MPa)
Values	125	0.22	32	13	125	0.10	0.5	20	0.05

Table 4 Back-analysis results for chainage K1 + 040 in the No. 4 diversion tunnel for the unsupported columnar joints

Date	Depth of EDZ at the sidewall		Mechanical properties of the joint between columns	
	Left	Right	ϕ_r^{j1} (°)	JRC ^{j1}
10 December, 2012	4	4.4	20.89	6.45
18 December, 2012	4.2	4.8	19.36	6.17
22 December, 2012	4.3	5.0	19.04	6.07
27 December, 2012	4.5	5.2	18.73	5.98

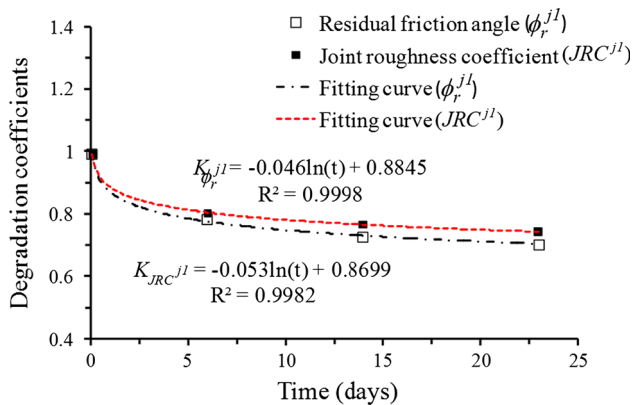


Fig. 23 Evolution of the parameters over time at chainage K1 + 040 in the No. 4 diversion tunnel

the models NN (n, h_1, h_2, m), while the second data set containing four data sets is used to test the performance of the obtained neural models. The evolutionary neural network is used to establish the non-linear mapping relationship between mechanical parameters (JRC^{j1} and ϕ_r^{j1}) and the depth of the EDZ for the first data set. The network thus obtained is NN (5, 47, 36, 7) and this network is used to back-analyse the depth of the EDZ at different times, to obtain the JRC^{j1} and ϕ_r^{j1} at these times (Feng et al. 2000, 2006; Feng and Hudson 2009). The back-analysis results are shown in Table 4. Because of the high non-linearity of the rock mass, the back-analysed results are usually non-unique, especially in the cases where there are several sets of parameters being estimated. Through sensitivity analysis, we determined the most sensitive parameters and then conducted global optimal search analysis, which can lead to reasonable solutions.

It can be seen from Table 4 that JRC^{j1} and ϕ_r^{j1} in unsupported columnar jointed rock mass show time-dependent decreases.

The variation of JRC^{j1} and ϕ_r^{j1} is plotted over time in Fig. 23. Here, the time in the abscissae with the time at which the evolution of EDZ is only influenced by the time, and not influenced by the excavation of tunnel face. It is found that both JRC^{j1} and ϕ_r^{j1} showed logarithmic deterioration over time, which indicates that the initial

deterioration rate is rapid, only to then decelerate rapidly. The fitted time-dependent degradation coefficients of JRC^{j1} and ϕ_r^{j1} are as follows:

$$K_{\phi_r^{j1}} = -0.046 \ln t + 0.8845 \tag{14}$$

$$K_{JRC^{j1}} = -0.053 \ln t + 0.8699 \tag{15}$$

5.2.2 Time-Dependent Coefficients of Supported Columnar Joint in the Deceleration Stage

The methods proposed in Sect. 5.2.1 are also used to obtain the time-dependent degradation coefficients for supported columnar joints during their deceleration stage at the same chainage. Data from 23 January to 2 February 2013 are selected for back-analysis (Table 5), during which time the columnar jointed rock mass have been supported.

It can be seen from the Fig. 24, that ϕ_r^{j1} for the supported columnar joints still have a significant time-dependent decrease, whereas JRC^{j1} is found to be less time-dependent. Therefore, only the time-dependent degradation coefficient of ϕ_r^{j1} is considered in the deceleration stage for these supported columnar joints.

$$K_{\phi_r^{j1}} = -0.019 \ln t + 0.9599 \tag{16}$$

The aforementioned results show that the time-dependent degradation coefficients of both supported and unsupported columnar jointed rock masses in the deceleration stage could be simplified to $K_{JRC}/K_{\phi_r} = a \ln t + b$ with a high correlation coefficient. The coefficients of JRC^{j1} and ϕ_r^{j1} both show a time-dependent decrease for the unsupported columnar joints, whereas for supported columnar jointed rock mass, only the coefficient of ϕ_r^{j1} shows any time dependency. The coefficient of ϕ_r^{j1} of the supported columnar jointed rock mass is also smaller than that for the unsupported case. It is thus demonstrated that the supported columnar jointed rock mass still exhibited time dependency, but the time-dependent degradation coefficient is less than that for the unsupported case. This correlated well with the regulation of EDZ evolution as evinced by field data.

Table 5 Back-analysis results of chainage K1 + 040 in the No. 4 diversion tunnel for supported columnar joints

Date	Depth of EDZ at the sidewall		Mechanical properties of the joint between columns	
	Left	Right	ϕ_r^{j1} (°)	JRC ^{j1}
23 January, 2013	5.2	6.5	21.35	6.40
25 January, 2013	5.3	6.5	21.10	6.39
28 January, 2013	5.3	6.6	20.85	6.38
2 February, 2013	5.4	6.6	20.06	6.35

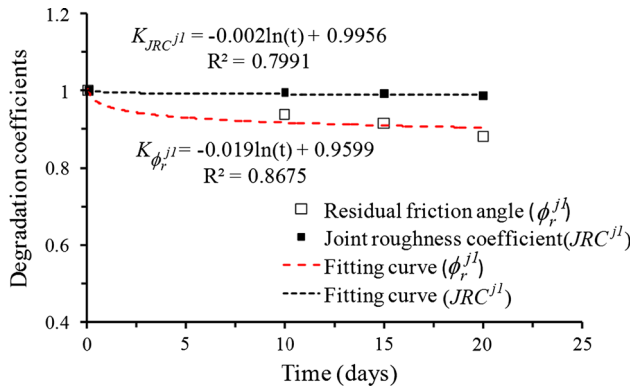


Fig. 24 Evolution of parameters over time of chainage K1 + 040 in the No. 4 diversion tunnel with support installed

5.2.3 Time-Dependent Coefficients of Unsupported Columnar Joint in the Steady State and Acceleration Stages

When the tunnel strain ε of the columnar jointed rock mass has reached threshold values of ε_s and ε_a , it enters the stabilization, and acceleration stages, respectively. Chainage K1 + 050 in the No. 5 diversion tunnel has experienced stabilization, and acceleration stages from 28 January to 14 March 2013 as shown in Fig. 19. The EDZ at chainage K1 + 050 is analysed to obtain the time-dependent degradation coefficient in the steady state and acceleration stages for unsupported columnar joints. The tunnel strain is determined as follows (Hoek 1998):

$$\text{Tunnel strain } \varepsilon_t = \text{wall displacement } \delta / \text{tunnel radius } r \tag{17}$$

In which, the tunnel radius can be determined as half of tunnel width. The threshold values of tunnel strain ε_s and ε_a could be obtained through dividing the displacements at the beginning of these two stages (Fig. 25) by the tunnel radius. Therefore, these two threshold values could be determined as 2.75×10^{-3} and 3.05×10^{-3} from in situ displacement data.

In the stabilization stage, the time-dependent degradation coefficient of ϕ_r^{j1} is as shown below:

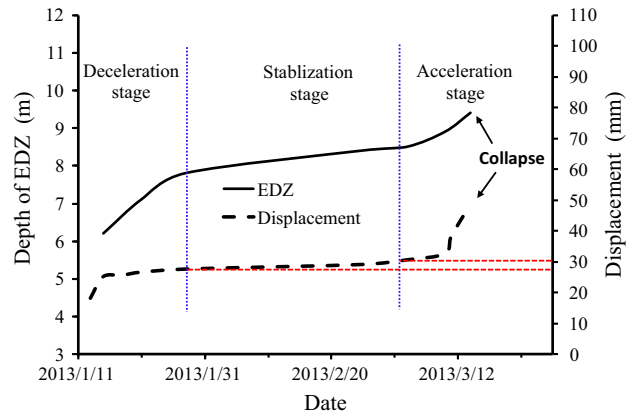


Fig. 25 In situ EDZ and displacement data of chainage K1 + 150 in the No. 5 diversion tunnel at different EDZ development stage

$$K_{\phi_r^{j1}} = -0.0076 \times t + 0.977 \tag{18}$$

In the acceleration stage, the time-dependent degradation coefficients of ϕ_r^{j1} and JRC^{j1} are as follows:

$$K_{\phi_r^{j1}} = 1 - 0.0002e^{0.3814t} \tag{19}$$

$$K_{JRC^{j1}} = 1 - 0.00015e^{0.3581t} \tag{20}$$

5.2.4 Summary of Time-Dependent Degradation Coefficients of the Columnar Joints

The degradation coefficients in the time-dependent constitutive model of columnar joints in different EDZ development stages are summarized below:

In the deceleration stage ($\varepsilon < 2.75 \times 10^{-3}$):

$K_{\phi_r^{j1}} = -0.046 \ln t + 0.8845$ for the unsupported surrounding rock mass.

$K_{JRC^{j1}} = -0.053 \ln t + 0.8699$ for the unsupported surrounding rock mass.

$K_{\phi_r^{j1}} = -0.019 \ln t + 0.9599$ for the supported surrounding rock mass.

In the stabilization stage ($3.05 \times 10^{-3} > \varepsilon \geq 2.75 \times 10^{-3}$):

$K_{\phi_r^{j1}} = -0.0076 \times t + 0.977$ for the unsupported surrounding rock mass.

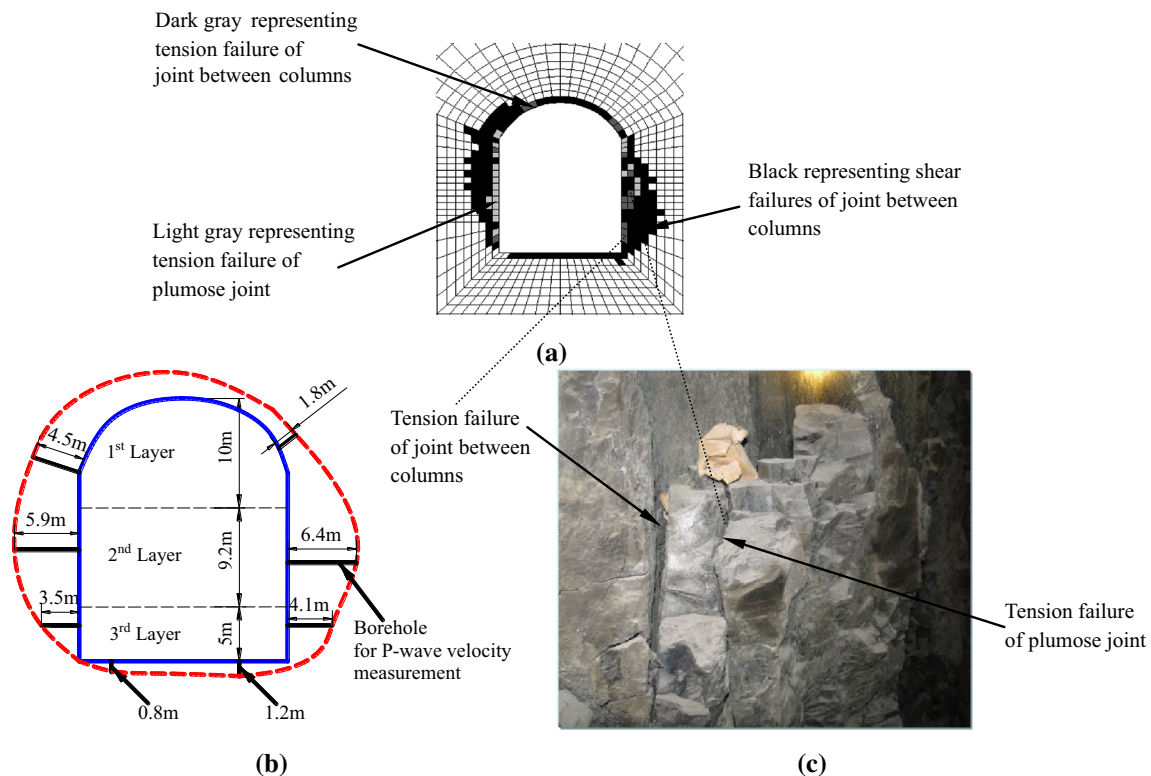


Fig. 26 Typical shape of EDZ of columnar joints by **a** numerical simulation and **b** in situ measurements, the typical failure pattern of EDZ of columnar joints by **a** numerical simulation and **c** in situ observation

In the acceleration stage ($\varepsilon \geq 3.05 \times 10^{-3}$):
 $K_{\phi_r^{j1}} = 1 - 0.0002e^{0.3814t}$ for the unsupported surrounding rock mass.
 $K_{JRC^{j1}} = 1 - 0.00015e^{0.3581t}$ for the unsupported surrounding rock mass.

6 Verification of the Time-Dependent Constitutive Model for Columnar Joints

6.1 Verification of the Failure Pattern

To verify the failure pattern of the columnar joints as obtained by SEM, this time-dependent constitutive model is used in numerical calculations. The results are shown in Fig. 26. It can be seen that the tensile failure of the joint between columns and the plumose joint mainly occurred at the surface of the surrounding rocks. However, shear failures of the joint between columns mainly occurred within the surrounding rocks. The results are in good agreement with SEM investigation shown in Figs. (11, 12, 13). The typical shape of the EDZ of columnar joints predicted by numerical simulation is also in good agreement with in situ measurements (the

arrangement of boreholes and corresponding test results at Chainage K1 + 040 in the No. 4 diversion tunnel are as shown in Fig. 22b).

6.2 Verification of the Time-Dependent Development of the EDZ

This time-dependent model is also used to simulate all monitored sections in the diversion tunnels on right bank to verify its suitability. First, the initial joint mechanics parameters (JRC^{j1} and ϕ_r^{j1}) at each monitoring section are obtained by back-analysis of the initial depth of the EDZ. Then, the aforementioned time-dependent degradation coefficients combining the initial JRC^{j1} and ϕ_r^{j1} values are substituted into the numerical simulation model. The depth of the EDZ at different times is calculated to compare that measured.

As shown in Figs. 27, 28 and 29, the numerical modelling results are in good agreement with the measured EDZ using the aforementioned time-dependent constitutive model for the columnar joints. This indicates that the model is accurate with regard to the simulation of time-dependent EDZ development.

Fig. 27 Comparison of in situ measurements and numerical simulation results for the EDZ at chainage K1 + 040 in the No. 4 diversion tunnel at right bank

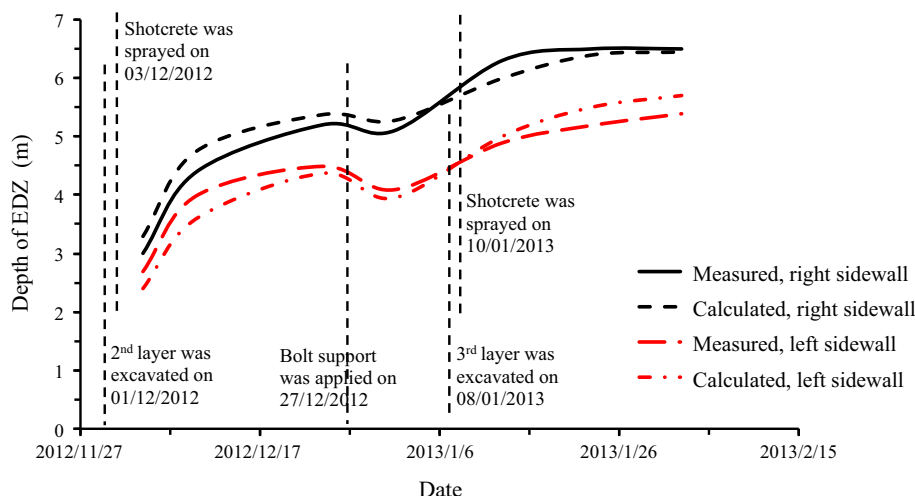
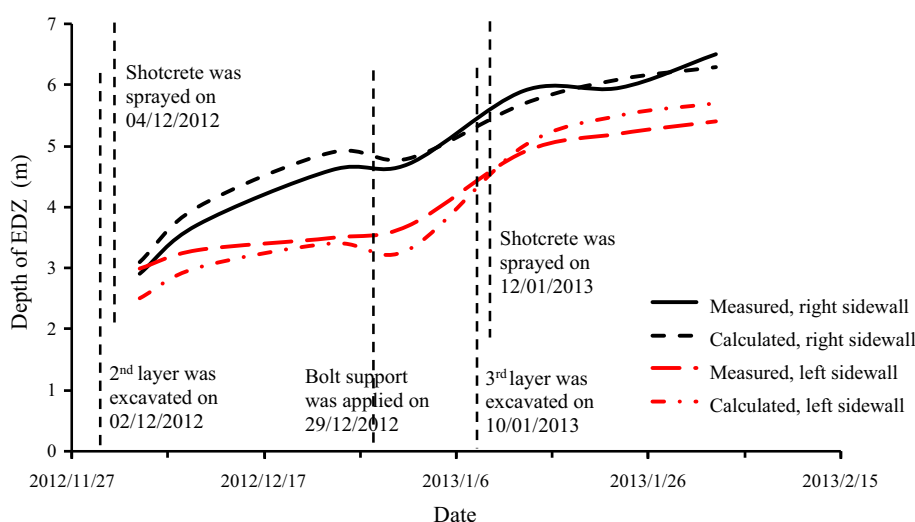


Fig. 28 Comparison of in situ measurements and numerical simulation results for the EDZ at chainage K1 + 050 in the No. 4 diversion tunnel at right bank



7 Discussions

7.1 Influence of Geo-Stress on the Time-Dependent Degradation Coefficient

It can be seen from the geological context outlined in Sect. 2 that the geo-stress on the right bank is higher than that on the left. Therefore, the method described in Sect. 5 is also used to calculate the time-dependent degradation coefficient on the left bank, to analyse the influence of geo-stress on the time-dependent degradation coefficient.

The mechanical properties of the columnar jointed rock mass over time on the left bank using back-analysis are shown in Table 6. The time-dependent degradation coefficient on the left bank for unsupported columnar jointed rock mass in deceleration stage is as follows:

$$K_{\phi_r^{jl}} = -0.0219 \ln t + 0.9894 \tag{21}$$

$$K_{JRC^{jl}} = -0.0199 \ln t + 0.9026 \tag{22}$$

Similarly, the time-dependent degradation coefficient on the left bank for supported columnar jointed rock mass in deceleration stage is:

$$K_{\phi_r^{jl}} = -0.0102 \ln t + 0.9875 \tag{23}$$

This time-dependent constitutive model is also used to simulate the monitored section of the left bank to verify its applicability. The results are shown in Figs. 30 and 31. The numerical modelling results are in good agreement with the measured EDZ. By comparing Eqs. (14–16) with (21–23), it can be found that when the geo-stress is lower, the corresponding time-dependent degradation coefficient is also lower, which demonstrates that the geo-stress is one of the

factors affecting the time-dependent degradation coefficient.

7.2 Long-Term Stability of the Diversion Tunnels

The diversion tunnels are temporary projects, and their main function is to divert the river after its closure during dam construction. Therefore, after completion of the dam, the role of the diversion tunnels came to an end. According to the construction plan for the Baihetan hydropower station, the dam will be completed in 2022. Therefore, the stability of the diversion tunnels within this period has become a concern.

The aforementioned time-dependent constitutive model for these columnar joints has been used to study the long-term development of the EDZ in the diversion tunnels until 2022. Figure 32 shows the variation of the EDZ in the diversion tunnels versus time elapsed since excavation. The results show that the final depth of the EDZ on the left and right banks is different. This may have arisen because of the different geo-stresses acting thereon. For the crown on the left bank, the depth of the EDZ is stable at 3.7 m after 90 days. For the sidewall on the left bank, the depth of the EDZ is stable at 4.5 m after 153 days. For the crown on the right bank, the depth of the EDZ is stable at 6.7 m after 122 days, and for the sidewall on the

right bank, the depth of the EDZ is stable at 7.6 m after 210 days.

The current support schemes for the columnar jointed rock masses are shown in Fig. 7. The anchor bolt at the sidewall has a length of 6 m, and at the crown, a length of 9 m. It can be seen from Fig. 33 that for the columnar jointed rock mass on the left bank, the ultimate depth of the EDZ is stable at 3.7–4.5 m, and the length of the anchor bolt covered the EDZ, allowing the diversion tunnel on the left bank to remain stable for the duration of the tunnel’s service life. For the columnar jointed rock mass on the right bank, the final depth of the EDZ is 6.7 m at the crown, and the 9 m anchor bolt also encompassed the EDZ; while for the sidewall, the 6 m anchor bolt could not span the 7.6 m EDZ. Therefore, it is recommended that further support be installed at the sidewall on the right bank. A 0.75 m lining is used to ensure sidewall stability of the diversion tunnel’s right bank. At time of writing, the diversion tunnel has been safely operating for the 6 months since 1 May, 2014.

It is found that the support system exerted a significant influence on the time-dependent mechanical behaviour of the columnar jointed rock masses as shown in Sect. 5.2.2. If the support is installed too early, the support system may sustain an excessive load. On the contrary, if the support installation is delayed, collapse may occur. Therefore, an optimal time between excavation and installation of supporting should be determined for future reference. And that, a support design method based on the depth of EDZ needs to be proposed to control the time-dependent crack propagation in the columnar jointed rock mass.

8 Conclusions

The stability of the columnar jointed rock mass, especially the time-dependent EDZ evolution of it, is one of the important problems for the Baihetan hydropower stations. Therefore, the time-dependent behaviour of such columnar jointed rock masses should be considered.

The development of crack propagation and the EDZ versus time is monitored during the excavation of the diversion tunnels. Through the field data, the crack

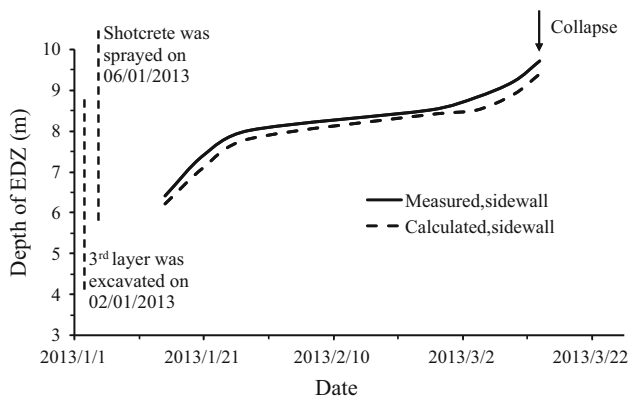


Fig. 29 Comparison of in situ measurements and numerical simulation results for the EDZ at the sidewall at chainage K1 + 050 in the No. 5 diversion tunnel at right bank

Table 6 Back-analysis results of chainage K0 + 315 in the No. 3 diversion tunnel on the left bank for supported columnar joints

Date	Depth of EDZ at sidewall (m)	Mechanical properties of the joint between columns	
		ϕ_r^{j1} (°)	JRC ^{j1}
16 January, 2013	1.3	26.6	8.23
24 January, 2013	1.5	23.19	7.06
22 February, 2013	1.6	21.48	6.39
3 March, 2013	1.67	21.22	6.30

Fig. 30 Comparison of in situ measurements and numerical simulation results for EDZ at chainage K0 + 315 in the No. 3 diversion tunnel

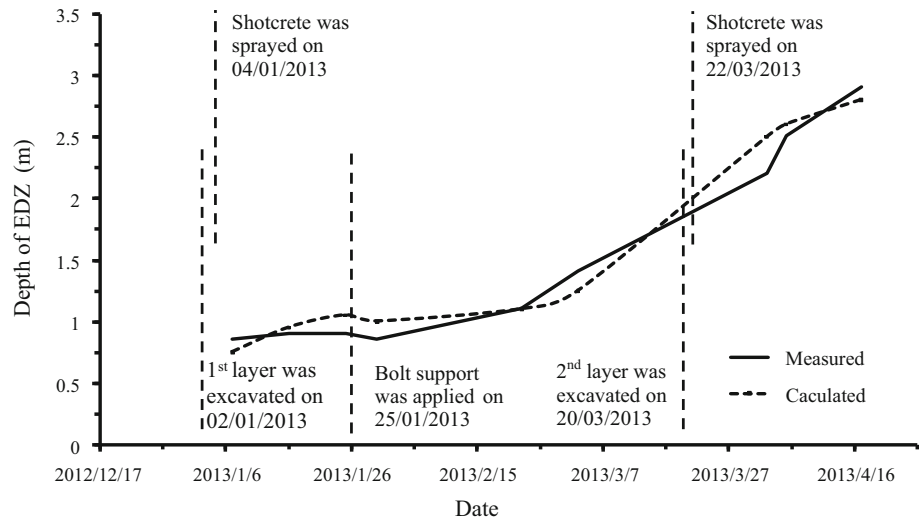


Fig. 31 Comparison of in situ measurements and numerical simulation results for EDZ at chainage K0 + 325 in the No. 3 diversion tunnel

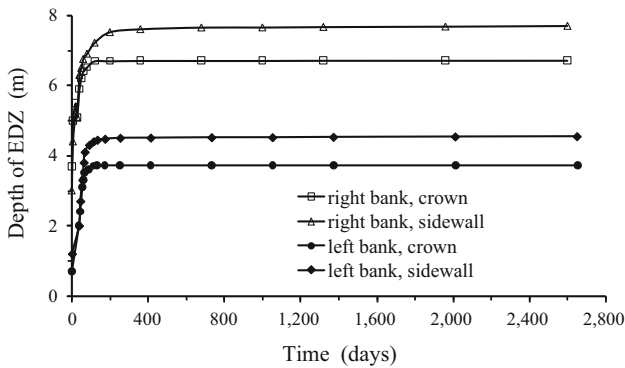
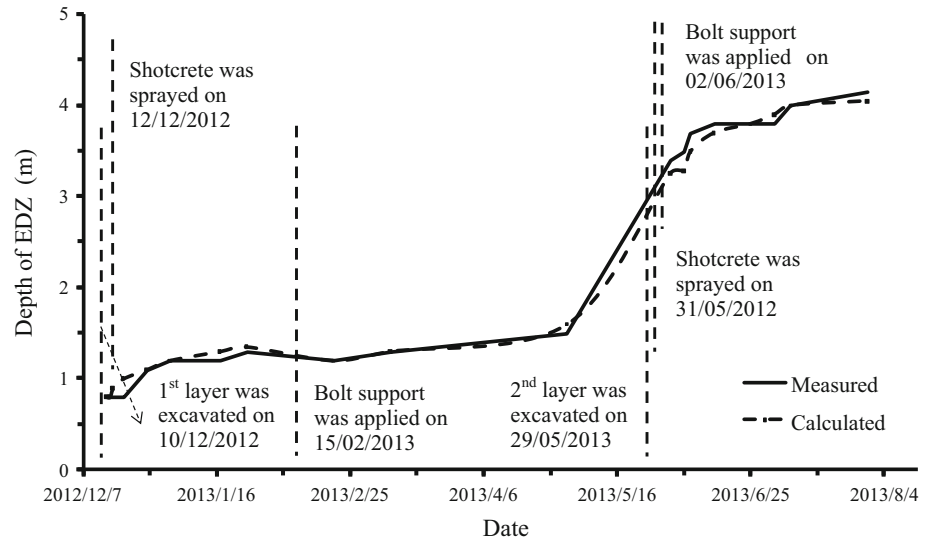


Fig. 32 Long-term evolution of the EDZ in a columnar jointed rock mass at different parts of the diversion tunnels on both left and right banks



Fig. 33 Diversion tunnels under safe operation

propagation and the depth of the EDZ is found to have increased over time. As the time-dependent crack propagation in the columnar jointed rock mass, the depth of EDZ increased and the strength of the columnar jointed rock mass decreased over time. However, the creep behaviour of the columnar jointed rock mass is not significant. The creep model could not be used here to solve the problem of the time-dependent development of EDZ.

A time-dependent strength model of the columnar jointed rock mass, considering multiple joints and anisotropic characteristic, is proposed. In this model, the time-dependent degradation coefficient of the roughness coefficient and residual friction angle of joint between the columns in the Barton–Bandis strength criterion is taken into account. An intelligent back-analysis method is adopted to obtain the unknown time-dependent degradation coefficients and initial mechanical properties in this constitutive model.

A numerical simulation is undertaken. The predicted failure patterns demonstrated that tensile failure of joint between columns and plumose joint mainly occurred at the surface of the surrounding rocks, while the shear failure of the joint between columns mainly occurred within the surrounding rocks, which verified the SEM results and in situ observation. In addition, this model is also used to simulate all monitored sections of the diversion tunnels. The numerical modelling results are in good agreement with the measured EDZ, indicating that this model has the ability to simulate the time-dependent EDZ development accurately.

Furthermore, the effects of the installed support system and the in situ stress field on the time-dependent degradation coefficients are also studied. The time-dependent degradation coefficient of the supported columnar jointed rock mass is lower than that of the unsupported rock mass. The time-dependent degradation coefficient of the left bank is found to be smaller than that of the right bank, which is caused by the higher geo-stress on the right bank.

Finally, long-term stability analysis of the diversion tunnels excavated in the columnar jointed rock mass is performed. For the columnar jointed rock mass on the left bank, the ultimate depth of the EDZ is stable at 3.7–4.5 m, and the 6 m length of the anchor bolt is sufficient to retain tunnel stability during the tunnel's service life. However, on the sidewall of the right bank, the 6 m anchor bolt could not encompass the 7.6 m EDZ. Therefore, the reinforced support of the sidewall on the right bank is recommended.

Because the time-dependent mechanical behaviour of such columnar jointed rock masses is greatly influenced by the support system, the optimal time between excavation and installation of supports should be determined by further research. And that, a support design method based on the depth of EDZ need to be proposed to control the time-

dependent crack propagation in the columnar jointed rock mass.

Acknowledgments Financial support from the National Natural Science Foundation of China under Grant no. 11232014 is gratefully acknowledged. The authors also thank Professors Y. L. Fan, X. D. Zhu, and A. C. Shi for their kind help for the field investigation, and the China Three Gorges Project Corporation for their technical assistance. In addition, the authors would like to acknowledge two anonymous reviewers for their helpful suggestions and comments.

References

- Barton N (1976) The shear strength of rock and rock joints. *Int J Rock Mech Min Sci Geomech Abstr* 13(9):255–279
- Belin S (1992) Application of backscattered electron imaging to the study of source rocks micro textures. *Org Geochem* 18:333–346
- Boidy E, Bouvard A, Pellet F (2002) Back analysis of time-dependent behavior of a test gallery in claystone. *Tunn Undergr Space Technol* 17(4):415–424
- Chambon P, Corte JF (1994) Shallow tunnels in cohesionless soil: stability of tunnel face. *J Geotech Eng* 120(7):1148–1165
- Côme B, Johnston P, Muller A (1984) Design and instrumentation of in situ experiments in underground laboratories for radioactive waste disposal. Taylor & Francis, London
- Cramer M, Dischler S, Erb D, Berlin G, Wittreich C, Bauer R (1987) Geomechanical testing development for the Basalt Waste Isolation Project. The 28th US symposium on rock mechanics (USRMS)
- Cruikshank KM (1996) Fractography: fracture topography as a tool in fracture mechanics and stress analysis. *J Struct Geol* 18(9):1182–1183
- Cundall PA (1988) Formulation of a three-dimensional distinct element model—Part I a scheme to detect and represent contacts in a system composed of many polyhedral blocks. *Int J Rock Mech Min Sci Geomech Abstr* 25(3):107–116
- Eberhardt E (2001) Numerical modeling of three-dimension stress rotation ahead of an advancing tunnel face. *Int J Rock Mech Min Sci* 38(4):499–518
- Erarslan N, Williams DJ (2013) Mixed-mode fracturing of rocks under static and cyclic loading. *Rock Mech Rock Eng* 46(5):1035–1052
- Fahimifar A, Monshizadeh TF, Hedayat A, Vakilzadeh A (2010) Analytical solution for the excavation of circular tunnels in a visco-elastic Burger's material under hydrostatic stress field. *Tunn Undergr Space Technol* 25(4):297–304
- Feng XT, Hudson JA (2009) Specifying the information required for rock mechanics modeling and rock engineering design. *Int J Rock Mech Min Sci* 47(2):179–194
- Feng XT, Zhang ZQ, Sheng Q (2000) Estimating mechanical rock mass parameters relating to the Three Gorges Project permanent shiplock using an intelligent displacement back analysis method. *Int J Rock Mech Min Sci* 37(7):1039–1054
- Feng XT, Chen BR, Yang CX, Zhou H, Ding XL (2006) Identification of visco-elastic models for rocks using genetic programming coupled with the modified particle swarm optimization algorithm. *Int J Rock Mech Min Sci* 43(5):789–801
- Glamheden R and Hökmark H (2010) Creep in jointed rock masses Main report of the SR-Can project. Swedish Nuclear Fuel and Waste Management Co(SKB), Stockholm, Sweden SKB Tech Rep R-06-94
- Goehring L, Lin ZQ, Morris SW (2006) Experimental investigation of the scaling of columnar joints. *Phys Rev E* 74(3):1–13

- Golshani A, Oda M, Okui Y, Takemura T, Munkhtogoo E (2007) Numerical simulation of the excavation damaged zone around an opening in brittle rock. *Int J Rock Mech Min Sci* 44(6):835–845
- Hart R, Cundall PA, Lemos J (1988) Formulation of a three-dimensional distinct element model—Part II mechanical calculations for motion and interaction of a system composed of many polyhedral blocks. *Int J Rock Mech Min Sci Geomech Abstr* 25(3):117–125
- Hatzor YH, Feng XT, Li SJ, Yagoda-Bira G, Jiang Q, Hu LX (2015) Tunnel reinforcement in columnar jointed basalt: the role of rock mass anisotropy. *Tunn Undergr Space Technol* 46(2):1–11
- Hoek E (1998) Keynote address: tunnel support in weak rock. In: *Proceedings of the symposium of sedimentary rock engineering, ISRM Regional Symposium, Taipei, Taiwan*, pp 281–292
- Hoek E, Brown ET (1997) Practical estimates of rock mass strength. *Int J Rock Mech Min Sci* 34(8):1165–1186
- Hommand-Etienne F, Hoxha D, Shao JF (1998) A continuum damage constitutive law for brittle rocks. *Comput Geotech* 22(2):135–151
- Hudson JA, Bäöckström A, Rutqvist J, Jing L, Backers T, Chijimatsu M, Christiansson R, Feng XT, Kobayashi A, Koyama T, Lee HS, Neretnieks I, Pan PZ, Rinne M, Shen BT (2009) Characterizing and modeling the excavation damaged zone (EDZ) in crystalline rock in the context of radioactive waste disposal. *Environ Geol* 57(6):1275–1297
- James JG (2009) Basalt columns: large scale constitutional supercooling? *J Volcanol Geotherm Res* 184:347–350
- James MD, Atilla A (1987) Surface morphology of columnar joints and its significance to mechanics and direction of joint growth. *Geol Soc Amer Bull* 99(5):5605–5607
- Jiang Q, Feng XT, Hatzor YH, Hao XJ (2014) Mechanical anisotropy of columnar jointed basalts: an example from the Baihetan hydropower station, China. *Eng Geol* 175:35–45
- Kaiser PK, Kim BH (2015) Characterization of strength of intact brittle rock considering confinement-dependent failure processes. *Rock Mech Rock Eng* 48(1):107–119
- Kamata G, Masimo H (2003) Centrifuge model test of tunnel face reinforcement by bolting. *Tunn Undergr Space Technol* 18(2):205–216
- Kemeny J (2003) The time-dependent reduction of sliding cohesion due to rock bridges along discontinuities: a fracture mechanics approach. *Rock Mech Rock Eng* 36(1):27–38
- King M, Myer L, Rezowalli J (1986) Experimental studies of elastic-wave propagation in a columnar-jointed rock mass. *Geophys Prospect* 34(8):1185–1199
- Krinsley DH, Pye K, Boggs S, Tovey NK (1998) Backscattered scanning electron microscopy and image analysis of sediments and sedimentary rocks. Cambridge University Press, Cambridge
- Kruhl JH (2013) Fractal-geometry techniques in the quantification of complex rock structures: a special view on scaling regimes, inhomogeneity and anisotropy. *J Struct Geol* 46:2–21
- Kuzmin VA, Skibitskaya NA (2011) Application of Fourier analysis of scanning electron microscopy images for studying variation features of reservoir properties of carbonate rocks at stages of catagenetic transformations. *J Surf Invest X-ray Synchrotron Neutron Tech* 5(5):1016–1020
- Lachenbruch AH (1962) Mechanics of thermal contraction cracks and ice-wedge polygons in permafrost. *Geol Soc Am Bull* 70:69
- Li SJ, Feng XT, Li ZH, Chen BR, Zhang CQ, Zhou H (2012) *In situ* monitoring of rockburst nucleation and evolution in the deeply buried tunnels of Jinping II hydropower station. *Eng Geol* 137:85–96
- Martin Z, Simon L, Dov B (2014) Growth of exfoliation joints and near-surface stress orientations inferred from fractographic markings observed in the upper Aar valley (Swiss Alps). *Tectonophysics* 626(20):1–20
- Mertens J, Bastiaens W, Dehandschutter B (2004) Characterization of induced discontinuities in the Boom clay around the underground excavations (URF, Mol, Belgium). *Appl Clay Sci* 26(4):413–428
- Mostafa S, Abolfazl T, Mohammad AM (2013) Time-dependent behavior of tunnel lining in weak rock mass based on displacement back analysis method. *Tunn Undergr Space Technol* 38:348–356
- Müller G (1998) Starch columns: analog model for basalt columns. *J Geophys Res* 103:15239–15253
- Nadimi S, Shahriar K, Sharifzadeh M, Moarefvand P (2011) Triaxial creep tests and back analysis of time-dependent behavior of Siah Bisheh cavern by 3-Dimensional distinct element method. *Tunn Undergr Space Technol* 26:155–162
- Nomikos P, Rahmamejad R, Sofianos A (2011) Supported axisymmetric tunnels within linear viscoelastic Burgers rocks. *Rock Mech Rock Eng* 44(5):553–564
- Park SH, Adachi T, Kimura M, Kimura M, Kishida K (1999) Trap door test using aluminum blocks. In: *Proceedings of the 29th Japan symposium of rock mechanics*, pp 106–111
- Pellet F, Roosefid M, Deleruyelle F (2009) On the 3D numerical modeling of the time-dependent development of the damage zone around underground galleries during and after excavation. *Tunn Undergr Space Technol* 24:665–674
- Rutqvist J, Börgesson L, Chijimatsu M, Hernelind J, Jing L, Kobayashi A, Nguyen S (2008) Modeling of damage, permeability changes and pressure responses during excavation of the TSX tunnel in granitic rock at URL. *Can Environ Geol* 57(6):1263–1274
- Sakurai S (1978) Approximate time-dependent analysis of tunnel supports structure considering progress of tunnel face. *Int J Numer Anal Met* 2(2):159–175
- Sellers EJ, Klerck P (2000) Modeling of the effect of discontinuities on the extent of the fracture zone surrounding deep tunnels. *Tunn Undergr Space Technol* 15(4):463–469
- Shao H, Schuster K, Sönneke J et al (2008) EDZ development in indurate clay formations—in situ borehole measurements and coupled HM modeling. *Phys Chem Earth* 33(Suppl 1):388–395
- Singh M, Rao KS, Ramamurthy T (2002) Strength and deformational behavior of a jointed rock mass. *Rock Mech Rock Eng* 35(1):45–64
- Sitharam TG, Shimizu N, Sridevi J (2001) Practical equivalent continuum characterization of jointed rock masses. *Int J Rock Mech Min Sci* 38(3):437–448
- Spry A (1962) The origin of columnar jointing, particularly in basalt flows. *J Geol Soc Austr* 8(2):191–216
- Sulem J, Panet M, Guenet A (1987) An analytical solution for time-dependent displacements in circular tunnel. *Int J Rock Mech Min Sci Geomech Abstr* 24(3):155–164
- Wang CY, Law KT, Sheng Q, Ge XR (2002) Borehole camera technology and its application in the Three Gorges project. In: *Proceedings of the 55th Canadian geotechnical and 3rd Joint IAHC-CNC and CGS groundwater specialty conferences, Niagara Falls, Ontario*, pp 601–608
- Yoshida H, Horii A (1992) Micromechanics-based model for creep behavior of rock arch. *Appl Rev* 45(8):294–303
- Zhang YH, Zhou HM, Zhong ZW (2011) *In situ* rock masses triaxial test system YXSW-12 and its application. *Chin J Rock Mech Eng* 30(11):2313–2320
- Zhao J (1997) Joint matching and shear strength, part A: joint matching coefficient. *Int J Rock Mech Min Sci* 34(2):173–178